

**IMAGING THE CERVICAL SPINAL CORD AND NERVE ROOTS
IN PATIENTS WITH SPINAL MUSCULAR ATROPHY
USING DIFFUSION TENSOR IMAGING**



MASTER'S THESIS TECHNICAL MEDICINE
MEDICAL IMAGING & INTERVENTIONS

BY
L. KUSTER

IMAGING THE CERVICAL SPINAL CORD AND NERVE ROOTS IN PATIENTS WITH SPINAL MUSCULAR ATROPHY USING DIFFUSION TENSOR IMAGING

MASTER'S THESIS TECHNICAL MEDICINE
MEDICAL IMAGING & INTERVENTIONS

BY
L. KUSTER

GRADUATION ON 11 DECEMBER 2015
UNIVERSITY OF TWENTE, ENSCHEDE

GRADUATION COMMITTEE

| | |
|-----------------------------|---|
| CHAIRMAN | PROF. DR. D.G. NORRIS <i>UNIVERSITY OF TWENTE, ENSCHEDE</i> |
| MEDICAL SUPERVISORS | PROF. DR. J. HENDRIKSE <i>UNIVERSITY MEDICAL CENTER UTRECHT</i> W. HAAKMA, MSc. (ADDITIONAL MEMBER) <i>UNIVERSITY MEDICAL CENTER UTRECHT</i> |
| TECHNICAL SUPERVISOR | DR. IR. B. TEN HAKEN <i>UNIVERSITY OF TWENTE, ENSCHEDE</i> |
| MENTOR | DRS. P.A. VAN KATWIJK <i>UNIVERSITY OF TWENTE, ENSCHEDE</i> |
| EXTERNAL MEMBER | DR. E.J.F.M. TEN BERGE <i>UNIVERSITY OF TWENTE, ENSCHEDE</i> |

THIS MASTER'S THESIS WAS CONDUCTED AT THE RADIOLOGY DEPARTMENT AND
THE NEUROLOGY DEPARTMENT OF THE UNIVERSITY MEDICAL CENTER UTRECHT,
WITH TECHNICAL SUPPORT FROM THE UNIVERSITY OF TWENTE

SUMMARY

Rationale Spinal muscular atrophy (SMA) is a disorder characterized clinically by axial and proximal muscle weakness and pathologically by degeneration of α -motor neurons, and is caused by the homozygous deletion of the survival motor neuron (SMN) 1 gene. SMN is important for RNA splicing and axonal transport, but the mechanisms that cause SMA are largely unknown. Reduced connectivity of motor neurons may be an important cause for muscle weakness in SMA. We hypothesize that reduced connectivity can be visualized in the spinal cord by using magnetic resonance imaging (MRI) and diffusion tensor imaging (DTI). Robust biomarkers for SMA severity and disease progression are needed because the relatively slow rate of disease progression has complicated the selection of clinical outcome measures for clinical trials. DTI could be helpful as a biomarker to evaluate efficacy of experimental treatment strategies. The aims of this study were to develop an acquisition protocol to visualize the spinal cord and the descending nerves and to gain more insight into the potential value of DTI as a biomarker for disease severity in SMA patients.

Methods We developed, optimized and validated an acquisition protocol for use in an observational cross-sectional pilot study. We included 8 patients with SMA types 2 and 3 and 14 healthy controls, who were scanned with the developed protocol. Two anatomical images and two diffusion weighted images were obtained. DTI data was corrected for subject motion and eddy current induced distortions, and diffusion tensors were calculated according to the weighted linear least squares (WLLS) procedure. Fiber tractography was performed and four diffusion parameters were computed of the cervical nerves (C5-C7): fractional anisotropy (FA), mean diffusivity (MD), axial diffusivity (AD), and radial diffusivity (RD). Cross sectional areas of the spinal cord and of the grey matter, and diameters of the anterior and posterior nerve roots were measured.

Results All diffusion parameters for nerves C5-C7 were significantly lower (FA: $p < 0.05$; MD, AD, RD: $p < 0.005$) in SMA patients than in healthy controls. Anatomical differences were found in grey matter to spinal cord area ratio and in anterior to posterior nerve root diameter ratio between an SMA patient and an age- and gender matched healthy control.

Conclusion We showed that it is possible to visualize the anatomical and microstructural properties of the cervical spinal cord and the descending nerve roots. To our knowledge we report the first clinical study that used DTI to investigate the anatomical and microstructural properties of the cervical spinal cord and nerves in patients with SMA. DTI can provide additional unique information regarding the pathophysiological mechanisms of SMA *in vivo*. This study provides a foundation for further exploration of DTI as a biomarker in SMA. Combining anatomical imaging, DTI and tractography, and correlating diffusion parameters with clinical outcome measures may prove a valuable contribution to better monitor the disease progression and therapeutic effect in SMA patients in the future.

TABLE OF CONTENTS

| | |
|--|----|
| Summary | 3 |
| List of Abbreviations | 6 |
| 1 Introduction, Objectives and Thesis outline..... | 7 |
| 1.1 Research objectives..... | 8 |
| 1.2 Thesis outline..... | 9 |
| 2 MRI acquisition protocol | 10 |
| 2.1 Introduction | 10 |
| 2.1.1 Basics of MRI..... | 10 |
| 2.1.2 Principles of diffusion | 11 |
| 2.1.3 Diffusion weighted imaging | 12 |
| 2.1.4 Diffusion tensor imaging | 13 |
| 2.1.5 Tractography | 14 |
| 2.1.6 Clinical focus..... | 15 |
| 2.2 Set of requirements..... | 15 |
| 2.3 Methods | 16 |
| 2.3.1 Data acquisition..... | 16 |
| 2.4 Results and discussion | 19 |
| 2.5 Conclusion | 23 |
| 3 Clinical study | 24 |
| 3.1 Introduction | 24 |
| 3.2 Method and materials..... | 25 |
| 3.2.1 Study design..... | 25 |
| 3.2.2 Study procedure | 26 |
| 3.2.3 Data processing and analysis | 26 |
| 3.2.4 Statistical analysis..... | 27 |
| 3.3 Results | 27 |
| 3.4 Discussion | 30 |

| | | |
|-------|---|----|
| 3.4.1 | Anatomical measurements | 30 |
| 3.4.2 | Tractography | 31 |
| 4 | Conclusion and future perspectives..... | 33 |
| 4.1 | Conclusion | 33 |
| 4.2 | Future perspectives..... | 33 |
| 4.2.1 | Protocol optimization | 33 |
| 4.2.2 | Clinical study | 35 |
| | Bibliography | 36 |
| | Appendix A. Approval Medical Ethical Committee of study ‘MR imaging of the spinal cord in patients with spinal muscular atrophy (SMA) and healthy controls (MuSIC study)’ | 43 |

LIST OF ABBREVIATIONS

| | |
|---------|---|
| 3D | three dimensional |
| AD | axial diffusivity |
| B_0 | applied external magnetic field |
| DTI | diffusion tensor imaging |
| DWI | diffusion weighted imaging |
| EPI | echo planar imaging |
| FA | fractional anisotropy |
| FOV | field of view |
| FVC | forced vital capacity |
| HFMSE | Hammersmith Functional Motor Scale Expanded |
| IC | informed consent |
| MD | mean diffusivity |
| mFFE | multi-echo fast field echo |
| MFM | Motor Function Measure |
| MRI | magnetic resonance imaging |
| NMJ | neuromuscular junction |
| PSIF | T2-enhanced steady-state gradient echo |
| RD | radial diffusivity |
| ROI | region of interest |
| SD | standard deviation |
| SMA | spinal muscular atrophy |
| SMA-FRS | SMA Functional Rating Scale |
| SMN | survival motor neuron |
| T | tesla |
| TE | echo time |
| TR | repetition time |
| TSE | turbo spin echo |

1 INTRODUCTION, OBJECTIVES AND THESIS OUTLINE

Hereditary proximal spinal muscular atrophy (SMA) is an autosomal recessive neuromuscular disorder with an incidence of 1 in 6.000-10.000 live births per year¹, and is an important genetic cause of infant mortality and morbidity.² The name ‘spinal muscular atrophy’ originates from the description by Guido Werdnig at the end of the 19th century, who documented the pathological findings of nerve root (‘spinal’) thinning in combination with muscle atrophy for the first time.³

SMA is characterized by degeneration of alpha motor neurons in the anterior horn of the spinal cord⁴, see Figure 1.1. The loss of these lower motor neurons leads to progressive muscle weakness of predominantly proximal and axial muscles, but distal and respiratory muscles can be affected as well. Clinically, SMA patients are classified into four types, according to the age of symptom onset and the highest motor function ever acquired.⁵ The majority of SMA patients experiences first symptoms in infancy or childhood and will have a mildly to severely reduced life expectancy.⁶

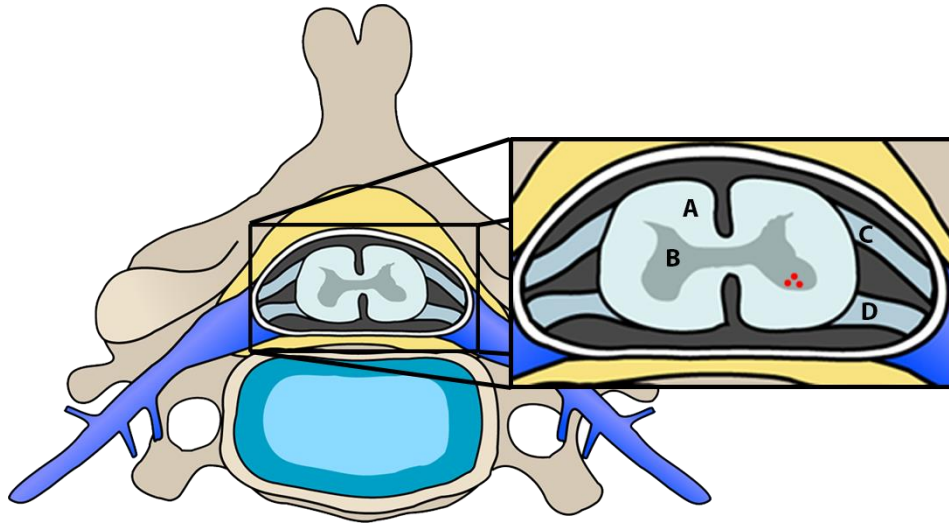


Figure 1.1 Schematic overview of a cervical vertebra. A indicates white matter, B indicates grey matter. C and D illustrate respectively the dorsal and ventral nerve root. The red dots represent the position of alpha motor neurons in the anterior horn of the spinal cord.

SMA is caused by a homozygous deletion of the survival motor neuron (SMN) 1 gene or by a hemizygous deletion and an additional disabling point mutation in the SMN1 gene, located on chromosome 5. Carrier frequency of an SMN1 deletion is 1 in 38-50.¹ SMN is a ubiquitously expressed protein that is known to function as part of several protein complexes involved in RNA splicing and axonal transport.⁷⁻¹¹ However, the mechanisms that cause SMA are still largely unknown.^{12,13}

In addition to lower motor neuron degeneration, the hallmark of the disease, neurophysiological studies have shown reduced H-reflexes in patients with SMA type 1, which may suggest reduced sensory-motor connectivity in the spinal cord.^{14,15} Furthermore, histological studies have shown an

abnormal architecture of the neuromuscular junction (NMJ) in tissue cultures of animal models¹⁶ and patients with SMA¹⁷, and an abnormal function of the NMJ has been found in patients with SMA types 2 and 3.¹⁸ Reduced connectivity of motor neurons may thus be an important cause of muscle weakness in SMA.

To provide more information on motor ability and clinical progression, several rating scales were devised.¹⁹⁻²⁴ A shortcoming of these scales is that they are not sufficiently sensitive to assess strength in very weak muscles, i.e. when movement is possible only if the influence of gravity is eliminated, and in muscles that are powerful enough to overcome gravity but are still weak.²⁵ Robust biomarkers for SMA severity and disease progression are needed because the relatively slow rate of disease progression has complicated the selection of clinical outcome measures for clinical trials. Biomarkers could be helpful to evaluate the efficacy of experimental treatment strategies. Therefore it is important to have a biomarker that can detect neuromuscular changes in more detail, preferably before these changes are reflected by muscle strength.

Specific magnetic resonance (MR) imaging techniques might be able to give more insight in structural changes and decreased connectivity of nerves *in vivo*. Earlier studies have used diffusion tensor imaging (DTI) to visualize the spine in healthy subjects.²⁶⁻³² These studies indicated several possible clinical applications, which have been broadly investigated since then. For example, DTI has revealed a loss of cervical cord tissue structure in multiple sclerosis (MS) patients.³³⁻³⁵ An earlier study of Oh et al. also showed that in patients with MS, DTI detects clinically relevant abnormalities beyond what can be detected by conventional MRI.³⁶ This phenomenon has been demonstrated in patients with amyotrophic lateral sclerosis (ALS) as well.³⁷ To our knowledge, the application of DTI in the spine to study motor neuron connectivity and nerve roots in patients with SMA has not been investigated before. When combining structural images with DTI, DTI could provide high resolution information about the anatomy and microstructural properties of the nerves. DTI could thus provide new insights in disease pathology *in vivo* and may be applied as a new biomarker for disease severity in SMA.

1.1 RESEARCH OBJECTIVES

This Master's Thesis focuses on developing a method for imaging the microstructural properties of the cervical spinal cord and its nerve roots, and on gaining more insight in the pathophysiological mechanisms of SMA and the applicability of DTI as a biomarker.

This leads to a methodological and a clinical research question:

1. *How can we image the morphology and microstructural properties of the cervical spinal cord and its nerve roots with the use of DTI?*
2. *What is the potential value of DTI as a biomarker for disease severity in SMA patients?*

To answer these questions, we will develop a scanning protocol that makes it possible to obtain information about the microstructural properties of the cervical spinal cord and its nerve roots. To investigate the potential value of DTI as a biomarker for disease severity, we will use this devised scanning protocol to collect and compare DTI data between SMA patients and healthy subjects.

1.2 THESIS OUTLINE

This first chapter described the clinical need for this project. A brief introduction on SMA was given, as well as an explanation of why there is a need for a suitable biomarker for disease severity and disease progression in patients with SMA. In Chapter 2, the development of an acquisition protocol for the cervical spinal cord will be described, containing different sequences to image the anatomy, morphology, and microstructural properties of the cervical spinal cord and its emerging nerve roots. Chapter 3 will describe the clinical study that is conducted using the developed scanning protocol. In Chapter 4 the main findings of this research project will be summarized and future perspectives will be discussed.

2 MRI ACQUISITION PROTOCOL

2.1 INTRODUCTION

2.1.1 Basics of MRI

Magnetic resonance imaging (MRI) is a technique based on the nuclear spin of a proton, which causes a magnetic moment. Normally the magnetic moments in a collection of protons will be randomly oriented, but when an external magnetic field (B_0) is applied the spin's magnetic moment tends to align with the direction of the applied field. This alignment is not perfect, a cone-shaped rotation around the axis of the applied field still occurs, the so-called Larmor precession (Figure 2.1A). The rate of precession is called the Larmor frequency and is influenced by the strength of B_0 . A collection of spins with the same Larmor frequency can be represented by a single net magnetization factor M , see Figure 2.1B. The net magnetization M consists of two components: M_{xy} in the transverse plane and M_z in the longitudinal plane (Figure 2.1C).

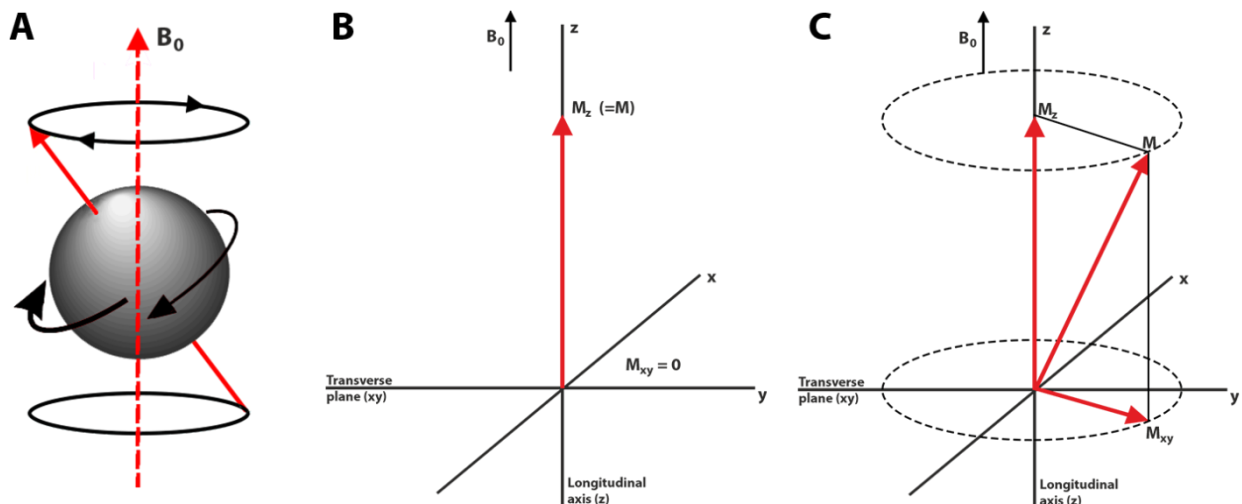


Figure 2.1 The Larmor precession of the nuclear spin of a proton along the axis of an applied magnetic field (B_0) is represented in A. B shows the net magnetization vector (M) in its static equilibrium state. M after excitation is shown in C, where the net magnetization consists of two components: M_{xy} in the transverse plane and M_z in the longitudinal plane. Figure based on Philips.³⁸

Due to Faraday's law of induction, only the magnetic component in the xy -plane can be detected.³⁹ In order to obtain information from the spins they must be knocked out of their relaxed, in-phase state along the z -axis, a process called spin excitation. This is done by applying a radio frequent (RF) 90° pulse that matches the Larmor frequency of the spins, see Figure 2.2. The initial net magnetization vector along the z -axis is deflected into the transverse xy -plane, where it precesses with the Larmor frequency (Figure 2.2A and Figure 2.2B). After excitation, relaxation occurs. In the relaxation process the spins realign with the external magnetic field along the z -axis, thereby emitting electromagnetic radiation in the form of an RF signal. Meanwhile, the magnitude of the net magnetization factor decreases due to

spin-spin interactions and magnetic field inhomogeneities in the xy -plane. Instead of one coherent Larmor frequency the spins now have their individual Larmor frequencies. This is called dephasing (Figure 2.2C).

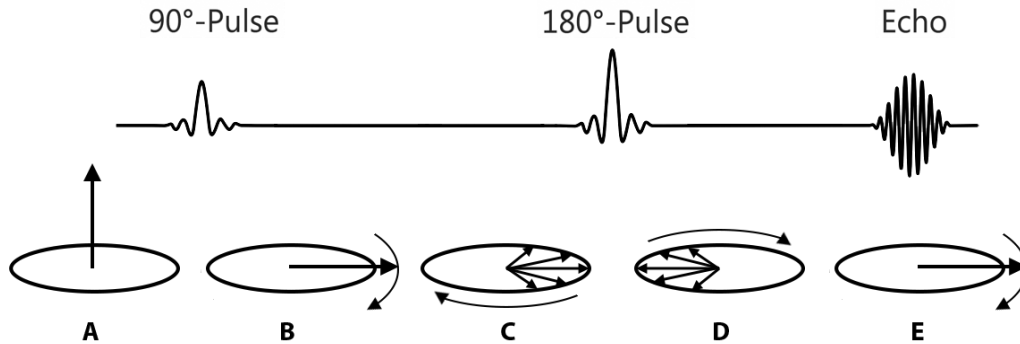


Figure 2.2 Dephasing of the magnetization factor and rephasing by a 180° pulse to form a spin echo (SE). (A) Net magnetization vector in static state. (B) Spin excitation after 90° pulse. (C) Dephasing of magnetization factor. (D) Rephasing of magnetization factor after 180° pulse. (E) Resulting spin echo signal.

The two dephasing processes are fundamentally different. Interactions between spins occur random, but inhomogeneities in the magnetic field are constant for a system, and can therefore be accounted for. By applying a 180° refocusing pulse, the individual spins are flipped around the x -axis. The spins continue precessing in the xy -plane, but because the effect of the field inhomogeneities is still the same, they are realigning, or rephasing (Figure 2.2D). The signal that occurs due to the rephasing of the spins is called the spin echo (SE), and is shown in Figure 2.2E.

2.1.2 Principles of diffusion

Diffusion is the random movement of water molecules, also called Brownian motion (Figure 2.3A).^{40,41} The amount of diffusion is quantified by the diffusion coefficient D . If diffusion can occur in all spatial directions, it is referred to as isotropic diffusion. Factors that influence diffusion are molecular weight, intermolecular interactions, and temperature.⁴² The underlying cellular microstructure of tissue influences the overall mobility of the diffusing molecules by providing barriers and by creating various individual compartments within the tissue.⁴³ The result is restricted diffusion. Restriction of diffusion can occur in all directions, which is shown in Figure 2.3B, or in one or two directions specifically, which is shown in Figure 2.3C and Figure 2.3D. When diffusion is restricted in one or two directions, it is referred to as anisotropic diffusion.

In the white matter of nervous tissue, axonal membranes and the myelin sheath primarily influence the direction of motion.⁴² This results in water molecules moving more freely parallel to the nerve fibers, and have its motion restricted perpendicular to the fiber tracts (Figure 2.3D).

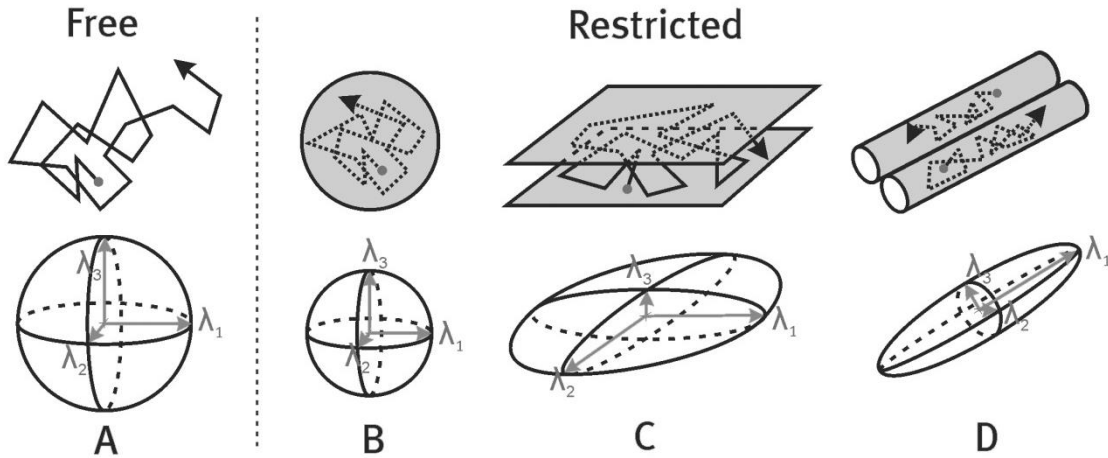


Figure 2.3 A schematic representation of free and restricted diffusion. The eigenvectors (grey arrows) represent directions of the principal axes and the corresponding eigenvalues (λ_1 , λ_2 , and λ_3) represent the magnitude of diffusion coefficients along these principal axes. (A) Free isotropic diffusion, equal probability of displacement in all directions, represented by a sphere ($\lambda_1 = \lambda_2 = \lambda_3$). (B) Isotropic hindered diffusion, equal probability of displacement in all directions, represented by a smaller sphere ($\lambda_1 = \lambda_2 = \lambda_3$). (C) Anisotropic diffusion, hindered in one direction, represented by a disc ($\lambda_1 \approx \lambda_2 \geq \lambda_3$). (D) = Anisotropic diffusion hindered in two directions, represented by an ellipsoid ($\lambda_1 \geq \lambda_2 \geq \lambda_3$).⁴⁴

2.1.3 Diffusion weighted imaging

Diffusion can be measured during an SE sequence by applying identical magnetic field gradients G before and after the 180° pulse. If a spin is stationary, these gradients have no effect: the spins will realign at the echo time (Figure 2.4A). However, if spins diffuse randomly between the application of the gradients, their precession frequency after the refocusing pulse will be different from the frequency before the pulse, and they will not realign perfectly (Figure 2.4B).

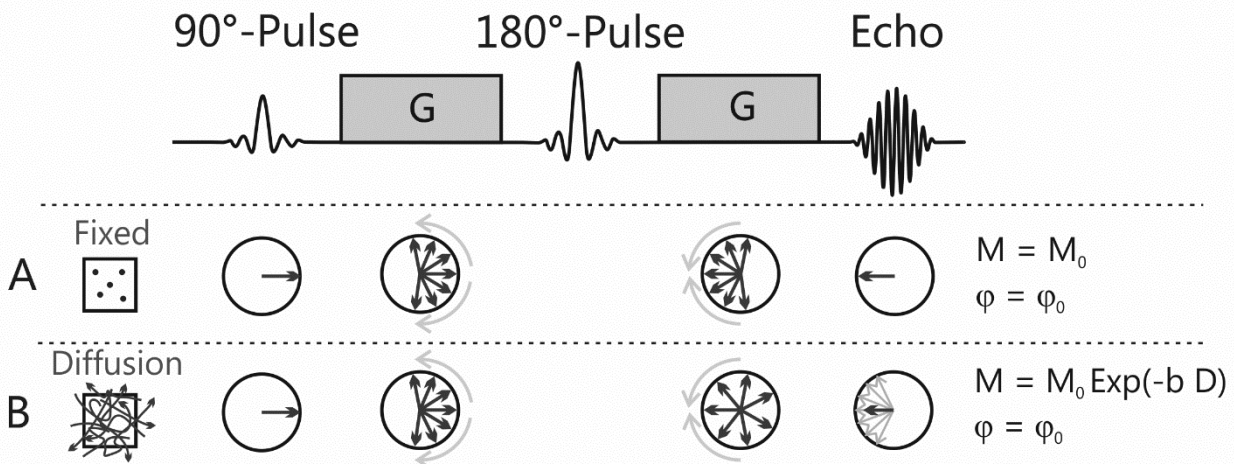


Figure 2.4 A schematic representation of a diffusion weighted spin echo (SE) pulse sequence and the resulting distributions of the phase of spins in the xy -plane of a voxel. Parameters: G = magnetic field gradient, M = net magnetization factor, ϕ = phase of magnetization factor, b = diffusion weighting factor, D = diffusion coefficient. (A) Fixed spins undergo the same dephasing and rephasing gradient, which results in no difference in phase and net magnetization. (B) Diffusing spins displace randomly in all directions. Each spin is subject to a different dephasing and rephasing gradient. Because of the random displacement there is no difference in net phase shift, but a decrease of net magnetization.⁴⁴

Imperfect realignment of the spins results in a lower echo amplitude, with the reduction depending on the strength and duration of the magnetic field gradient (b-value), and the diffusion coefficient D. The relation between the initial net magnetization vector M_0 and the resulting net magnetization vector M_b is shown in Equation 2.1.

$$M_b = M_0 e^{-bD} \quad (2.1)$$

2.1.4 Diffusion tensor imaging

In anisotropic structures, diffusion cannot be characterized by a single scalar, but requires a tensor, $\underline{\mathbf{D}}$.

$$\underline{\mathbf{D}} = \begin{matrix} D_{xx} & D_{xy} & D_{xz} \\ D_{yx} & D_{yy} & D_{yz} \\ D_{zx} & D_{zy} & D_{zz} \end{matrix} \quad (2.2)$$

The diffusion tensor fully describes molecular mobility in three directions, and the correlation between these directions. As can be seen in Equation (2.2), the diffusion coefficient needs to be measured in at least six independent directions. This is done by applying multiple diffusion encoding gradients. A visual representation of the tensor can be done by a sphere. When the diffusion is isotropic, the tensor is a perfect sphere, but when diffusion has a main direction, the tensor becomes an ellipsoid. The ellipsoid is defined by three eigenvectors and three eigenvalues (λ_1, λ_2 , and λ_3), which correspond respectively to the principal diffusion directions and associated diffusivities⁴⁵ (see Figure 2.3D).

Several scalars were introduced to characterize diffusion anisotropy.⁴⁶ The diffusivity along the principal axis is called the axial diffusivity (AD). AD is equal to eigenvalue λ_1 . The diffusivities along the two axes perpendicular to the principal axis are often averaged to form the radial diffusivity (RD).

$$RD = \frac{\lambda_2 + \lambda_3}{2} \quad (2.3)$$

The mean diffusivity (MD) is the average of all eigenvalues.

$$MD = \frac{\lambda_1 + \lambda_2 + \lambda_3}{3} \quad (2.4)$$

The degree of anisotropy in the tissue is described by the fractional anisotropy (FA) index.⁴⁷

$$FA = \sqrt{\frac{3}{2} \frac{\sqrt{(\lambda_1 - MD)^2 + (\lambda_2 - MD)^2 + (\lambda_3 - MD)^2}}{\sqrt{\lambda_1^2 + \lambda_2^2 + \lambda_3^2}}} \quad (2.5)$$

For an isotropic medium diffusion is equal in all directions, so FA is 0. For a cylindrically symmetric anisotropic medium, FA is 1.

To visualize the three-dimensional information in two dimensions and to make the tensor data easier to read, in 1999, Pajevic and Pierpaoli suggested to use a color-coded scheme.⁴⁸ The most basic red-green-

blue (RGB) color-coded scheme attributes a color for each orientation of the fibers: fibers running left-right are visualized in red, fibers running anteriorly-posteriorly are visualized in green and fibers running inferiorly-superiorly are visualized in blue. Figure 2.5 shows the different steps in defining a tract and color indication.

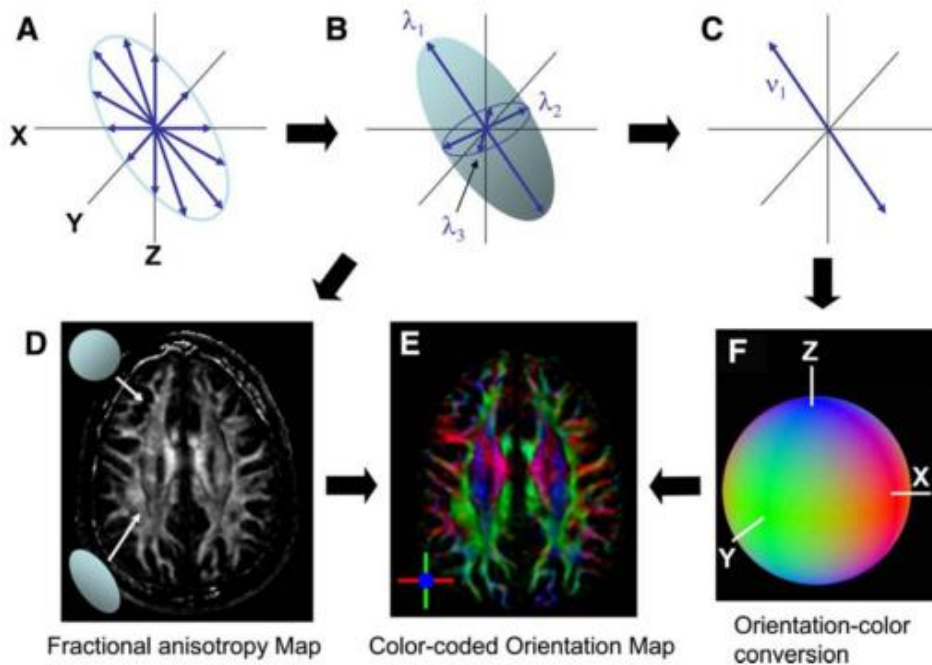


Figure 2.5 The use of a color-coded scheme to visualize fiber orientation. Diffusion measurements in several directions are performed (A), from which a diffusion ellipsoid is estimated (B). The information of all estimated ellipsoids is combined in an anisotropy map (D), in which regions with isotropic diffusion (spherical) are dark and regions with anisotropic (elongated) diffusion are bright. The eigenvector (v_1) with the largest eigenvalue (λ_1) in the estimated ellipsoid, is assumed to represent the local fiber orientation (C). For each voxel a color can be allocated, according to information about the orientation in 3D (F). Combining the color information (F) with the anisotropy map (D) results in a color-coded orientation map (E).⁴⁹

The color-coded FA maps are sufficient for visualizing DTI data in two dimensions. However, when neuronal connections are to be observed, a three-dimensional representation of the data is preferred.

2.1.5 Tractography

A commonly used method for giving a three-dimensional representation of DTI data is tractography, see Figure 2.6. With tractography, fiber systems are reconstructed based on the eigenvector fields in the DTI data.⁴⁹ First, a seed region of interest (ROI) is manually or automatically selected. Then, streamlines are propagated based on the assumption that the orientation of the longest axis of the diffusion tensor (v_1) represents the local fiber orientation. Different ending conditions for a streamline can be selected. For example; ending conditions can be based on when a region of low anisotropy is reached and no coherent fiber organization is present, or when the angular change of the fiber tract is too large. Specific threshold values for ending conditions can be appointed before tractography is performed.^{40,49-}

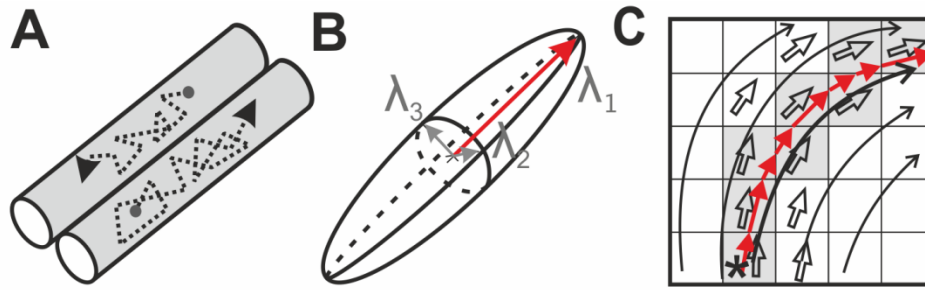


Figure 2.6 Principles of fiber tractography. Anisotropic diffusion in an environment with strongly aligned fibers (A) is represented by an ellipsoid (B). From the ellipsoid the fiber direction is determined for each voxel, represented by the open arrows (C). Fiber tractography starts in the voxel indicated with (*), called the seed, in panel C. Actual fibers are represented by the curved black lines. The connected voxels are shaded gray. The result of tractography is shown by the red arrows.⁵²

2.1.6 Clinical focus

DTI has been used extensively for imaging pathologies of the brain.⁵³⁻⁵⁷ Several neuronal pathologies that are expressed in the spinal cord have been imaged with DTI as well. Examples of these pathologies are amyotrophic lateral sclerosis (ALS),^{37,58-60} multiple sclerosis (MS),^{36,61-63} and neuromyelitis optica (NMO).^{64,65} To our knowledge, DTI of the spinal cord in patients with SMA has not been investigated before. In this chapter we focus on the acquisition protocols that are needed to visualize the pathology of SMA in the spinal cord. We explain for each clinical characteristic of SMA which MRI protocol should be developed. Per protocol different parameter settings are studied.

2.2 SET OF REQUIREMENTS

Factors affecting image quality include the MRI hardware and software configuration, acquisition sequences, and scanning parameters.⁶⁶ Optimizing image acquisition parameters is an essential step for producing high-quality DTI scans. In our set-up the scanner and coil are fixed conditions. A framework for an acquisition sequence for DTI on the cervical spinal cord is available at the University Medical Center Utrecht (UMCU).

In this study we aimed to develop a new protocol to image the cervical spinal cord and nerve roots at 3.0T by optimization of the acquisition parameters. The protocol should meet the following requirements:

1. Identify the microstructural properties of the grey and white matter in the spinal cord;
2. Identify the microstructural properties of the nerve roots exiting the spinal canal;
3. Anatomical imaging of the grey and white matter in the spinal cord;
4. Anatomical imaging of the cervical nerve roots exiting the spinal canal.

2.3 METHODS

2.3.1 Data acquisition

Between February 2015 and July 2015 nine healthy volunteers were scanned. All of the MRI was performed on a 3.0T MR system (Ingenia, Philips Healthcare, Best, The Netherlands) using a 20-channel phased-array dStream HeadNeckSpine coil.

Four different acquisition sequences were optimized to meet the set of requirements, two anatomic sequences and two diffusion-weighted sequences:

1. A diffusion weighted SE sequence ('DTI myelum') with a high in-plane resolution is developed to investigate the microstructural properties of the grey and white matter in the spinal cord, and the anterior and posterior nerve roots;
2. A T2-weighted multi-echo fast field echo sequence ('mFFE') is optimized to make an anatomical distinction between the grey and white matter in the cervical spinal cord;
3. A T2-weighted contrast enhanced gradient echo sequence ('PSIF') is optimized to depict the anterior and posterior nerve roots in the axial plane;
4. A diffusion weighted SE sequence ('DTI roots') with an isotropic voxel size is developed to study the microstructural properties of the descending lower cervical nerves.

Characteristics for all acquisition sequences are shown in Table 2.1.

Table 2.1 Characteristics for all acquisition sequences.

| Protocol name | DTI myelum | mFFE | PSIF | DTI roots |
|-------------------------------|-------------|----------------|--------------|-------------|
| Plane | Axial | Axial | Axial | Coronal |
| Echo time TE (ms) | 96 | 7.8 (2 echo's) | 6.1 | 62 |
| Repetition time TR (ms) | 1657 | 700 | 12 | 6442 |
| Flip angle (degrees) | 90 | 28 | 26 | 90 |
| Field of view (mm x mm) | 240x60 | 160x160 | 200x181 | 280x120 |
| Acquisition matrix | 240x59 | 248x246 | 332x297 | 112x46 |
| Voxel size (mm x mm x mm) | 1.0x1.0x5.0 | 0.65x0.65x5.0 | 0.6x0.61x0.5 | 2.5x2.5x2.5 |
| Slices | 10 | 17 | 160 | 30 |
| b-value (s/mm ²) | 800 | NA | NA | 800 |
| Number of gradient directions | 10 | NA | NA | 10 |
| Acquisition time (min) | 05:50 | 05:47 | 05:49 | 10:06 |

The experiments around three specific acquisition parameters are elucidated below.

Experiment 1: Different b-value. The b-value measures the degree of diffusion weighting applied and characterizes the gradient pulses (strength, duration, and spacing) used in the acquisition sequence. A higher b-value shows more diffusion weighting but also more noise. A higher b-value is achieved by increasing the gradient amplitude and duration by widening the interval between gradient pulses.

To determine the optimum b-value for imaging the diffusion in the cervical spine, two healthy volunteers both received two DTI examinations with different b values of 0, 100, 800, 1200, and 1600 seconds per mm². Other acquisition parameters were according to the DTI myelum protocol described in Table 2.1.

Experiment 2: Different sensitivity encoding (SENSE). In clinical practice, realistic arrays of coils that completely cover the sample are overlapping. Their sensitivity regions are extending beyond the field of view (FOV), causing aliasing (Figure 2.7).

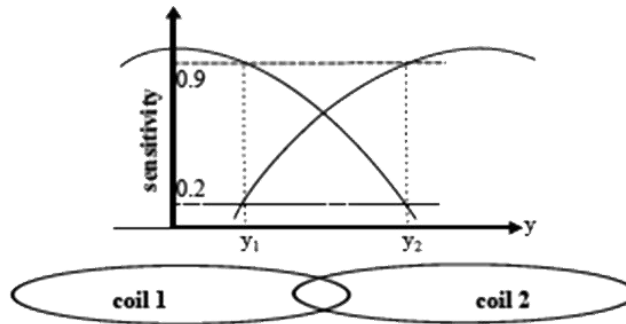


Figure 2.7 Example of two coils and their overlapping sensitivity regions. The dotted square represents the field of view (FOV).⁶⁷

The sensitivity encoding method combines coil images in the spatial domain in such a way that aliasing is averted. This is possible because the difference in proximity of surface coil elements to different tissues means that the expected relative signal intensity from different coil elements can be calculated. An example of the principle of sensitivity encoding is shown in Figure 2.8. The reduction of the number of phase encoding steps with respect to full Fourier encoding is described by the SENSE reduction factor, R. So, if every other acquired line is removed from the spatial domain, then R is 2.

The influence of applying SENSE on the images is tested for both diffusion sequences. For the ‘DTI myelum’ sequence, SENSE reduction factors of 1.0, 1.4, and 1.7 were tested on one healthy volunteer. The ‘DTI roots’ sequence is tested for SENSE factors 2.0 and 2.5. All other acquisition parameters were kept the same, as described in Table 2.1.

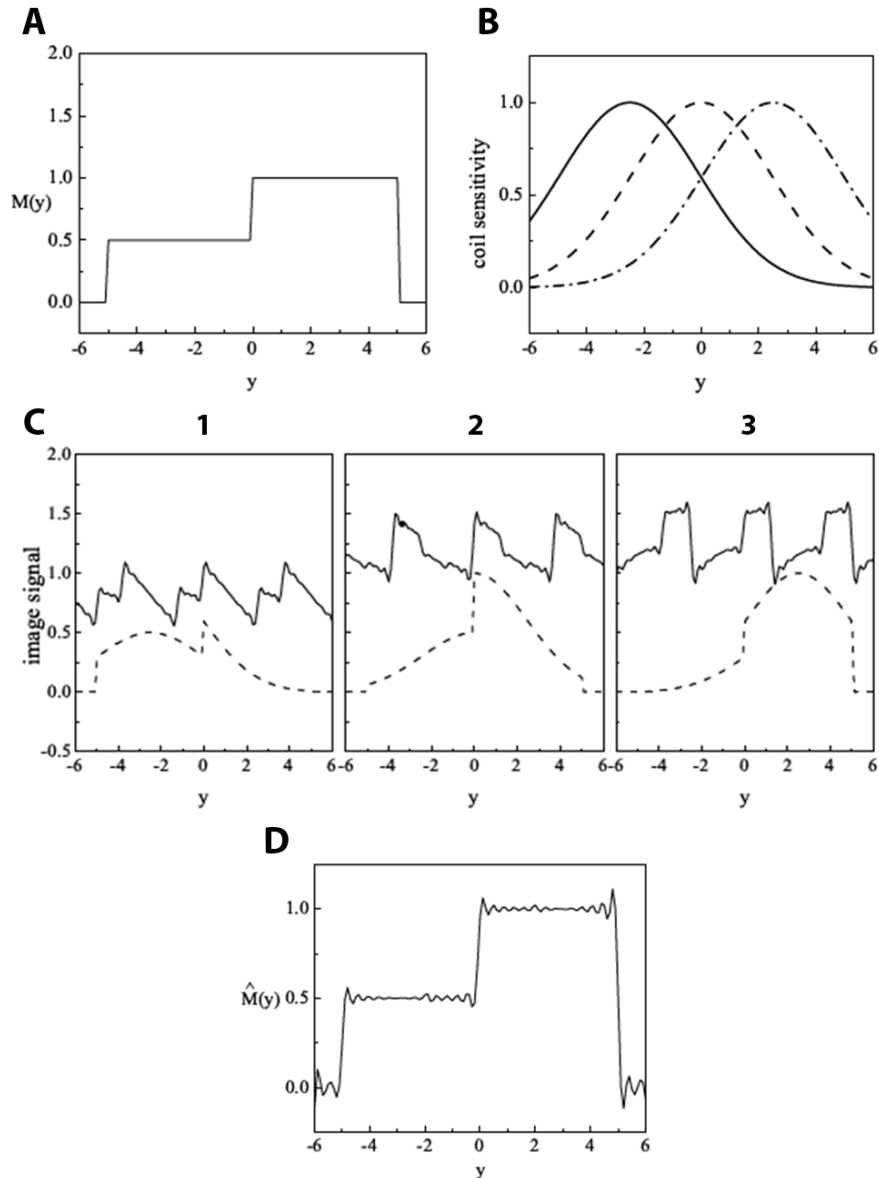


Figure 2.8 Example of the principle of sensitivity encoding. (A) The applied magnetic field M over a distance y , in this case the length of the field of view (FOV). (B) The sensitivity profiles for a three-coil example, shown as solid curve for coil (1), dashed curve for coil (2), and dot-dashed curve for coil (3). (C) The measured signal intensity for the three-coil example, shown for each coil separately. The dashed lines are the non-aliased intensity profiles for each coil. The solid lines are the sum of the signal intensity for each coil. (D) The reconstructed magnetization \hat{M} of the signal shown in (A), using the known relative coil sensitivities to the FOV to do a reconstruction. Modified from Brown et al.⁶⁷

Experiment 3: Different gradient enhancement. Different gradient enhancement options are available to increase either the voltage or the currents that are applied on the gradient coils. The first enhancement option ('gradient maximum') links two power supplies in a parallel way, thereby causing the current to go up. A higher current applied on the gradient coil results in a steeper slope of the gradient. A steeper slope means faster image acquisition. However, due to the parallel linking the applied voltage goes down, so the strength of the gradient will be lower. In practice this results in lower maximum b-values that can be measured.

The second enhancement option ('gradient enhanced') puts two power supplies in series. Thereby the applied voltage goes up, resulting in a higher gradient amplitude and thereby a higher b-value that can be achieved. However, due to the linking in series the applied current goes down and the gradient slope will be more gradual. Also, the extra voltage causes the system to heat up quickly, so it needs more time to cool down between the SE sequences, causing a longer total acquisition time.

The options 'gradient enhanced' and 'gradient maximum' were compared for the DTI roots sequence on one healthy volunteer.

2.4 RESULTS AND DISCUSSION

In this chapter, three important acquisition parameters for diffusion imaging were compared, and two diffusion acquisition sequences and two anatomical acquisition sequences were developed.

Experiment 1.

Figure 2.9 shows images of the same slice, but the diffusion measurements are acquired with different b-values. It shows that the higher the b-value, the lower the SNR. b-values of 1200 s/mm^2 and 1600 s/mm^2 do not result in a diffusion signal that is high enough to distinguish the diffusion from the noise. Therefore, a b-value of 800 s/mm^2 is chosen as the optimum b-value for imaging the cervical spinal cord. A b-value of 100 s/mm^2 instead of 0 s/mm^2 as a reference value is chosen to cancel out the high diffusion signal that is caused by cerebrospinal fluid (CSF) at $b = 0$. Otherwise the CSF signal could interfere with the relatively low diffusion signal measured from the spine.

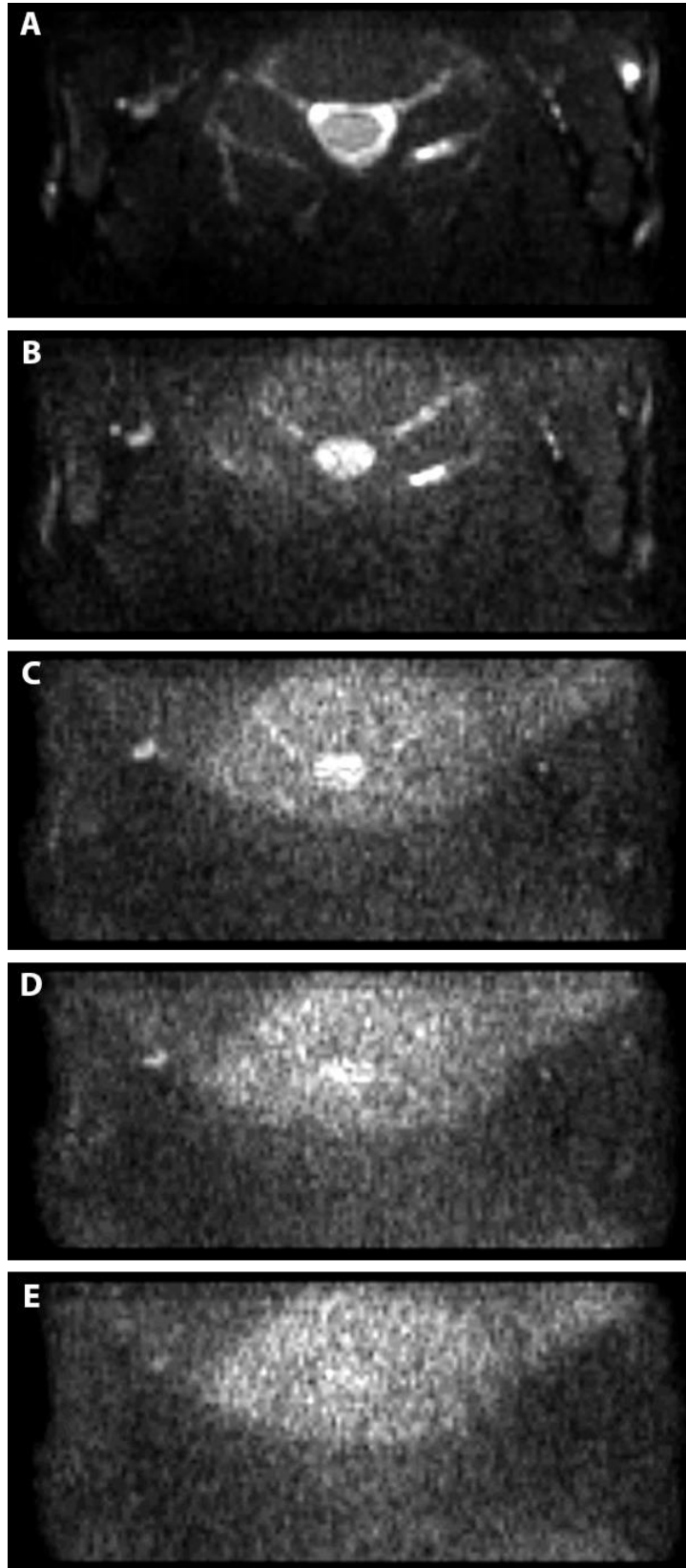


Figure 2.9 Signal intensity in DTI myelum sequence, using different b values. An axial slice of the neck on level C5 is shown, with (A) b is 0 s/mm^2 , (B) b is 100 s/mm^2 , (C) b is 800 s/mm^2 , (D) b is 1200 s/mm^2 , (E) b is 1600 s/mm^2 .

Experiment 2.

The effect of SENSE on the DTI myelum sequence and the DTI roots sequence is shown in Figure 2.10 and Figure 2.11 respectively. Figure 2.10 shows that applying SENSE improves the diffusion signal, up to a point where too much information is removed from the spatial domain and SENSE causes its own artefacts, known as nonuniform noise. This can be seen at the top part in Figure 2.10C. Therefore a SENSE factor of 1.4 is chosen for the DTI myelum sequence.

The images of the DTI roots sequence in Figure 2.11 show this nonuniform noise as well. Some SENSE was needed to acquire enough diffusion signal from the descending nerves. With the improved diffusion signal for these nerves taken into consideration, a concession is done on the nonuniform noise and a SENSE factor of 2 is chosen for the DTI roots sequence.

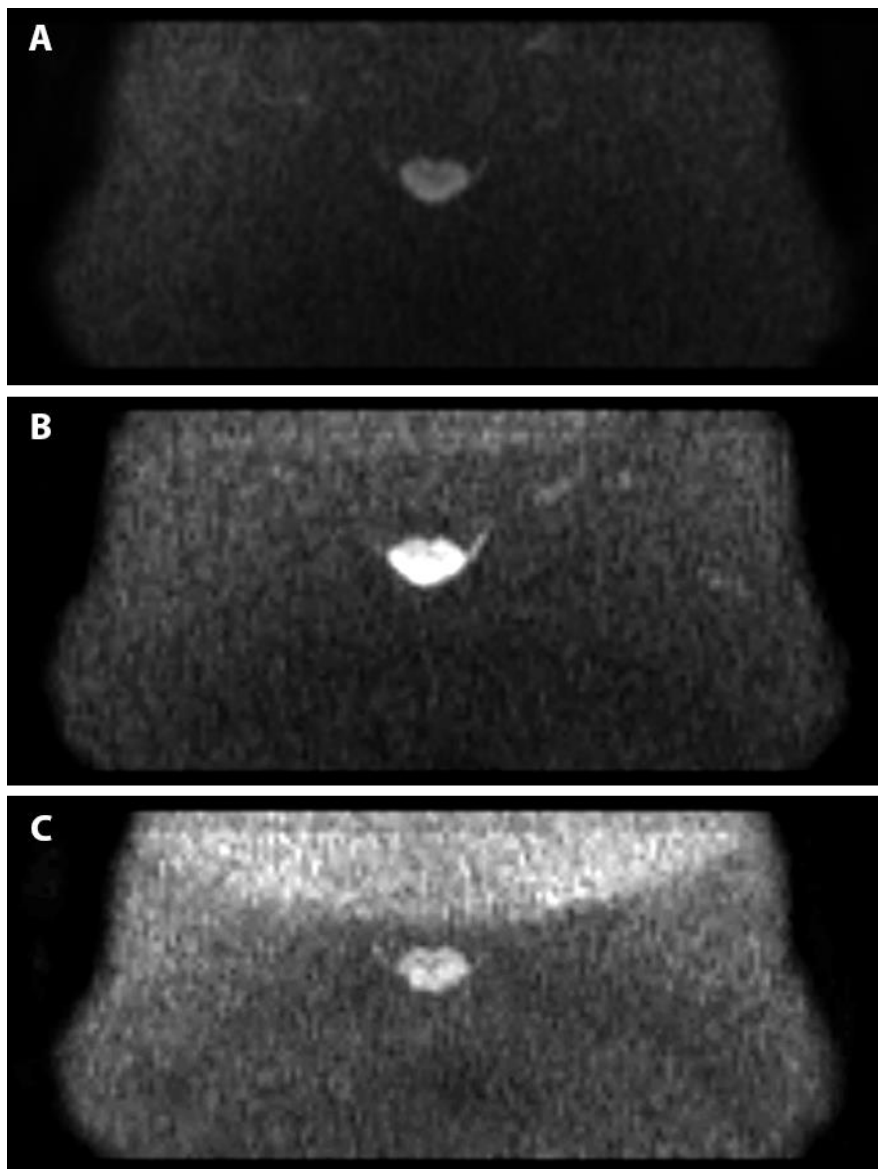


Figure 2.10 Signal intensity in DTI myelum sequence using different SENSE factors. An axial slice of the neck at level C5 acquired with a b-value of 800 s/mm² is shown. In (A) SENSE is 1, in (B) SENSE is 1.4, in (C) SENSE is 1.7.

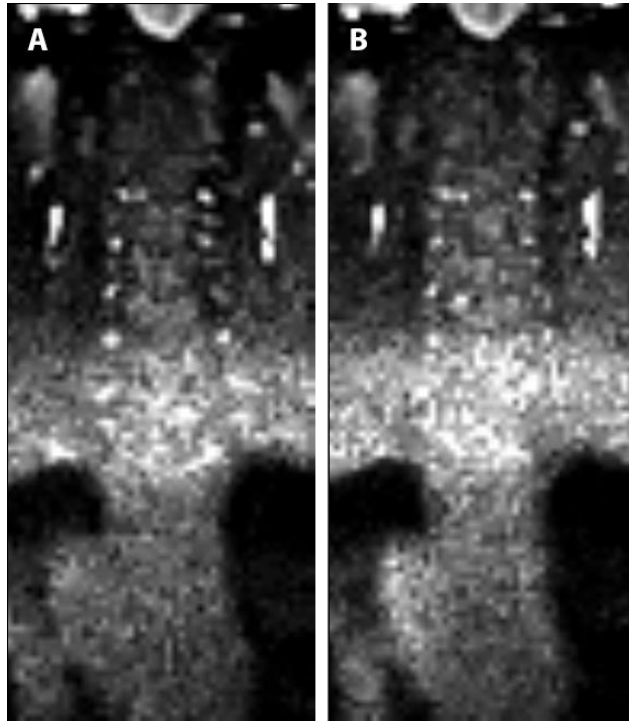


Figure 2.11 DTI roots acquisition sequence with varying SENSE factors. A sagittal slice of the cervical nerve roots and part of the lungs acquired with a b -value of 800 s/mm^2 is shown. In (A) SENSE is 2, and in (B) SENSE is 2.5.

Experiment 3.

The decision on the optimal gradient enhancement option is based on the fiber tractography of the spinal cord and the nerves. Figure 2.12A shows the tractography of the DTI roots sequence when the ‘gradient maximum’ option is used. The tractography of the DTI roots sequence with the use of the ‘gradient enhancement’ option is shown in Figure 2.12B. Tractography results show longer and thicker fibers (see Figure 2.12B) when the ‘gradient enhancement’ option is used. Therefore, despite the longer acquisition time, we chose to use the ‘gradient enhancement’ acquisition parameter in the DTI roots sequence.

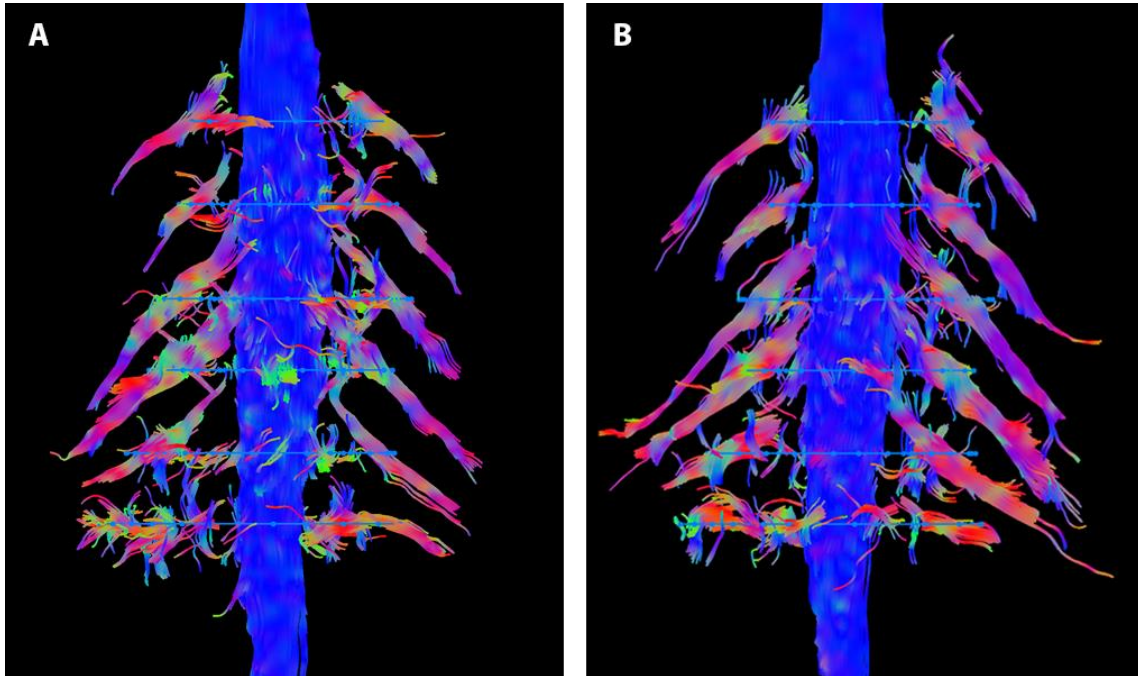


Figure 2.12 Tractography of the cervical spinal cord and its descending nerves. A = 'gradient maximum' used in acquisition protocol, B = 'gradient enhanced' used in acquisition protocol. The horizontal blue lines represent the regions of interest (ROIs) from which seed voxels are taken to perform tractography. The ROIs have the same position for both A and B.

2.5 CONCLUSION

To image the morphology and microstructural properties of the cervical spinal cord and the descending nerves, an acquisition protocol consisting of four different sequences was developed. Two specific DTI acquisition sequences were developed, optimized and validated in healthy control subjects. The DTI myelum sequence has its focus on the spinal cord itself, the focus of the DTI roots sequence is on the cervical nerve roots and nerves. To support possible findings in the DTI sequences, two anatomical sequences were developed and optimized as well, with the mFFE sequence focusing on the distinction between grey and white matter in the myelum, and the PSIF sequence focusing on the nerve roots originating from the myelum. Combining all sequences resulted in an acquisition protocol with which it is possible to visualize the cervical spinal cord and the descending nerve roots.

3 CLINICAL STUDY

3.1 INTRODUCTION

In the previous chapter, a method to study the morphology and microstructural properties of the cervical spinal cord and its nerve roots has been described. We used this method to study *in vivo* motor connectivity in patients with SMA in a clinical study, named ‘MR imaging of the spinal cord in patients with spinal muscular atrophy (SMA) and healthy controls’ (acronym: MuSIC).

In Chapter 1 the relevance of this clinical study is highlighted. With an incidence of 1 in 6.000-10.000/year¹ and a mildly to severely reduced life expectancy, SMA is the most common genetic cause of infant mortality and morbidity.² SMA is characterized by degeneration of alpha motor neurons in the anterior horn of the spinal cord due to shortage of SMN protein.^{4,12} The loss of lower motor neurons leads to progressive muscle weakness of proximal and axial muscles. Clinically, SMA patients are classified into four types, according to the age of symptom onset and the highest motor function ever achieved.⁵ The classification of the four different types is given in Table 3.1.^{68,69}

Table 3.1 Clinical classification of SMA in four different types

| SMA type | Age of onset | Highest motor function ever achieved |
|----------|----------------------|--|
| Type 1 | <6 months | Never learn to sit |
| Type 2 | 6-18 months | Learn to sit without help, never be able to walk independently |
| Type 3 | 18 months – 30 years | Learn to walk without help, lose ambulation later in life |
| Type 4 | >30 years | May have difficulties running, or climbing stairs |

To provide more information on motor ability and clinical progression, several rating scales were devised.¹⁹⁻²¹ The SMA Functional Rating Scale (SMA-FRS) is an easily administered ordinal rating scale based on 10 aspects of activities of daily living, with each subset scored from 0 (fully dependent) to 5 (fully independent)^{70,71}; the Medical Research Council (MRC) scale uses the ability to move against gravity and resistance as most important parameter to document muscle strength of 38 separate muscles, given a score ranging from 0 (no contraction) to 5 (normal strength); the Motor Function Measure (MFM) tests standing and transfers, and axial, proximal and distal motor function using 32 tasks, scored from 0 (cannot initiate task) to 3 (performs task fully and ‘normally’)⁷²; the Expanded Hammersmith Functional Motor Scale (HFMSE) scores motor skills on 33 items using a 3 point (0-2) Likert scale.¹⁹

As previously mentioned, a shortcoming of these scales is that they are not sufficiently sensitive to assess strength in very weak muscles.⁷³ Robust biomarkers for SMA severity and disease progression are needed because the relatively slow rate of progression has complicated the selection of clinical outcome measures for clinical trials. Biomarkers could be helpful to evaluate the efficacy of experimental

treatment strategies. Therefore, it is important to have a biomarker that can detect neuromuscular changes in more detail, preferably before these changes are reflected by muscle strength. Specific MRI protocols might be able to give more insight in structural changes and decreased connectivity *in vivo*.

The objective of this study is to provide insight in the pathophysiological mechanisms of SMA *in vivo*, and to investigate to what extent DTI can be used as a biomarker for disease severity in SMA patients.

3.2 METHOD AND MATERIALS

3.2.1 Study design

An observational cross-sectional pilot study at the UMC Utrecht was established to investigate motor connectivity *in vivo* in patients with SMA. The MuSIC study was approved by the local medical ethics research committee. From August 2015 to November 2015, eight SMA patients type 2 and 3 with a mean age of 51 years (range 17-73 years), and fourteen age- and gender-matched healthy controls (mean age of 55 years, range 31-72 years) were included. Inclusion and exclusion criteria are listed below.

Inclusion criteria

- Age 12 years or older;
- Capable of thoroughly understanding the study information given;
- Given written informed consent.

Additional inclusion criteria for SMA patients:

- A diagnosis of SMA type 2 or 3, diagnosed on clinical grounds and confirmed by homozygous deletion of the SMN1 gene.

Additional inclusion criteria for healthy controls:

- Controls are healthy and do not have any history of SMA or other neurological disorders.

Exclusion criteria

- Tracheostomy, tracheostomal ventilation of any type, (non)-invasive ventilation;
- Presence of pronounced swallowing disorders or orthopnea (which make it dangerous to lie supine in the MRI scanner);
- Forced vital capacity (FVC) >15% postural change between sitting and supine, or symptoms of nocturnal hypoventilation (recurrent morning headaches, night sweats, orthopnea);
- Contra-indications for MRI (e.g. a pacemaker, claustrophobia, pregnancy);
- Previous trauma or surgery of the (cervical) spine.

3.2.2 Study procedure

After written informed consent was obtained, the general medical history was assessed. The SMA-FRS was filled out and a neurological examination took place, assessing the MRC score, MFM, and HFMSE. Also, an FVC measurement was performed, in sitting and supine position.

All subjects were examined with the same 3.0 Tesla MR system (Ingenia, Philips Medical Systems, Best, The Netherlands) using a 20-channel phased-array dStream HeadNeckSpine coil. Two morphological images and two diffusion weighted images were obtained to visualize the cervical spinal cord, the nerve roots and the descending nerves, and to quantify diffusion parameters. The acquisition protocol consisted of the four sequences mentioned in Chapter 2.

3.2.3 Data processing and analysis

Anatomical measurements were performed using Philips DICOM viewer R3.0 (Philips Medical Systems, Best, The Netherlands). Cross sectional areas of the cervical spinal cord and of the grey matter were measured in the mFFE data by manually drawing a smoothed polygon around these structures (Figure 3.1A). Diameters of the anterior and posterior nerve roots were measured in the PSIF data by placing a caliper orthogonally to the nerve root in the middle between the spinal nerve and the myelum (Figure 3.1B).

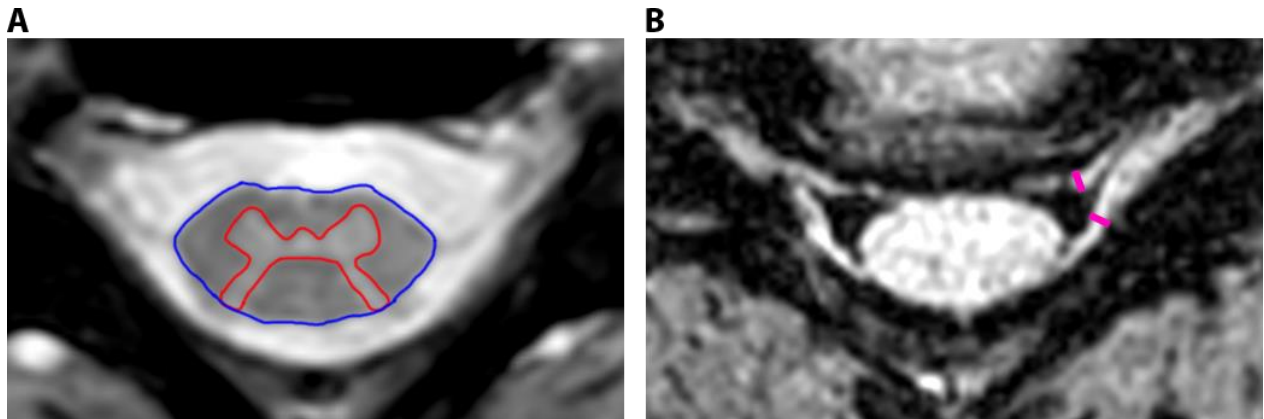


Figure 3.1 Methods for anatomical measurements. (A) shows the cross sectional area of the cervical spinal cord in blue, and the cross sectional area of the grey matter in red. (B) shows two calipers placed orthogonally to the nerve root in the middle between the spinal nerve and the myelum in pink.

DTI data was processed using ExploreDTI.⁷⁴ First, data was corrected for subject motion and eddy current induced distortions, and echo planar imaging (EPI) deformations.^{75,76} Second, diffusion tensors were calculated according to the weighted linear least squares (WLLS) procedure⁷⁷, using 10.000 iterations and 20.000 data samples. Third, DTI based fiber tractography was performed with a fractional anisotropy (FA) threshold of 0.2-1.0, minimum fiber length of 10 mm and a threshold angle of 30 degrees. Tractography analysis consists of two parts: (1) a mask was generated to use as a seed region of interest (ROI) for tractography analysis on the DTI myelum data; (2) seed ROIs in the DTI roots data were drawn manually, with the starting seed placed at the point where the anterior and posterior nerve root

converge to form the spinal nerve, and the end seed placed so that tractography analysis over a nerve tract length of 6 slices is performed. Four diffusion parameters were computed: fractional anisotropy (FA), mean diffusivity (MD), axial diffusivity (AD), and radial diffusivity (RD).

3.2.4 Statistical analysis

A Mann-Whitney U test was used to compare the diffusion data of the patient group with the diffusion data of the healthy control group. Statistical analyses were performed in IBM SPSS Statistics 22 (IBM Corp., Armonk, NY, USA). A p-value less than 0.05 was considered to be statistically significant.

3.3 RESULTS

The results of the anatomical sequences are represented as a case report. In Figure 3.2 two examples of the images obtained with the mFFE sequence are shown. Figure 3.2A shows the distinctive grey matter 'H-figure' in a healthy control, where in Figure 3.2B the 'H-figure' in an SMA patient is depicted. Cervical spinal cord cross sectional area was 88.9 mm² in the control and 86.3 mm² in the patient. The grey matter area measured 21.2 mm² in the control and 16.7 mm² in the patient. This results in a grey matter to cervical spinal cord ratio of 0.24 for the healthy control and 0.19 for the patient.

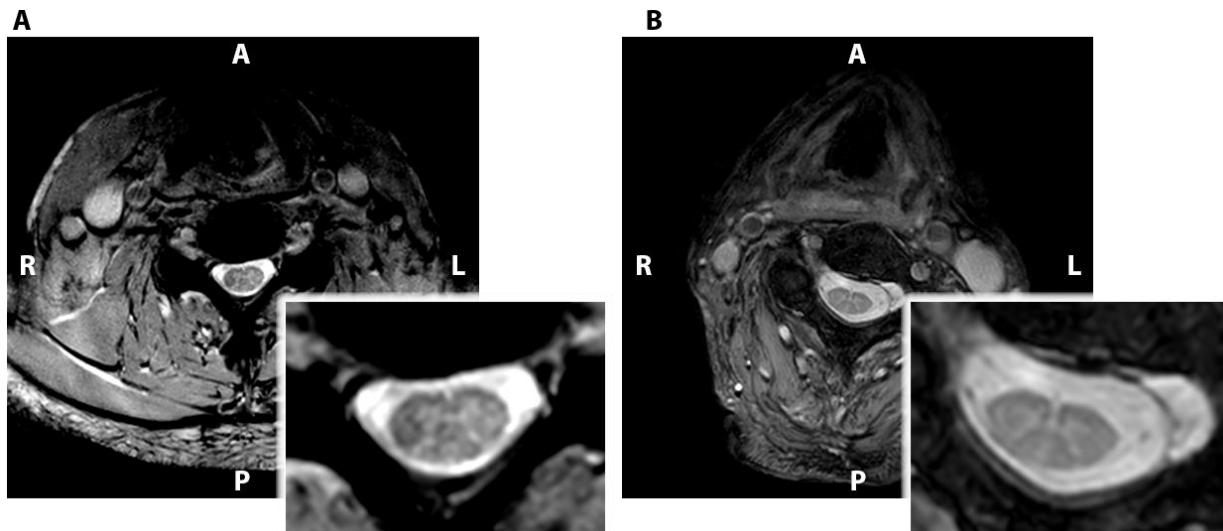


Figure 3.2 mFFE images of (A) a healthy control (male, 59 years) and (B) an SMA patient (male, 57 years). The enlargement in the frame shows the cervical myelum and the grey matter (light grey) within the white matter (dark grey), surrounded by cerebrospinal fluid (white).

Two examples of the acquired images using the PSIF sequence are shown in Figure 3.3. The anterior and posterior nerve roots of a healthy control are shown in Figure 3.3A. The mean diameter of the left and right anterior nerve root is 1.31 mm, the mean diameter of the left and right posterior nerve root is 1.30 mm. This results in an anterior to posterior nerve root ratio of 1.00 for this healthy control. Figure 3.3B shows the nerve roots in an SMA patient. The mean measured diameter of the left and right anterior nerve root is 0.79 mm and the mean diameter of the left and right posterior nerve root is 1.41 mm. The anterior to posterior nerve root ratio is 0.56 for this patient.

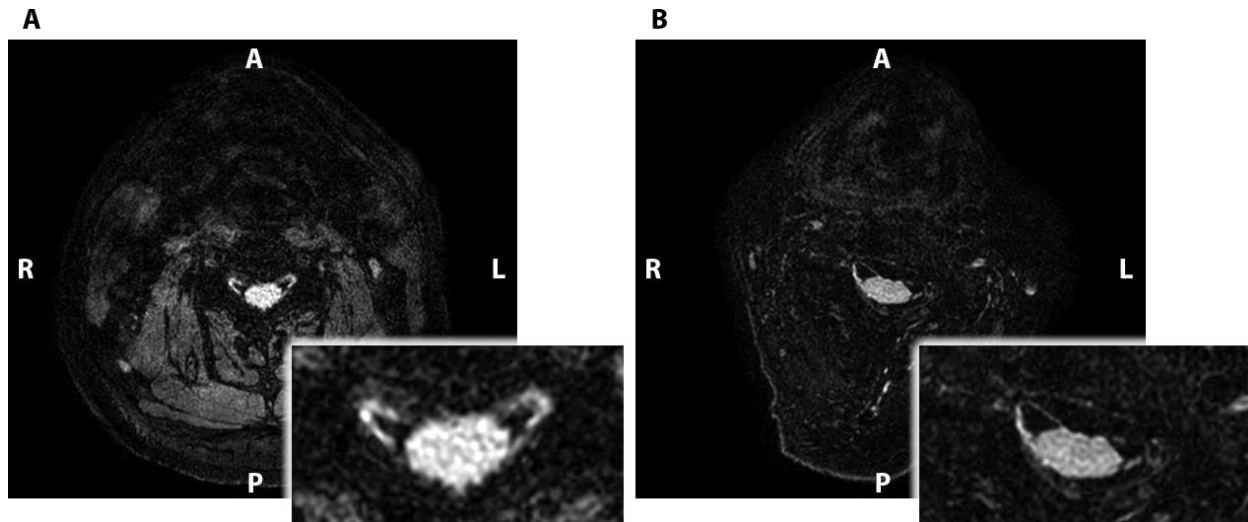


Figure 3.3 PSIF images of (A) a healthy control (male, 59 years) and (B) an SMA patient (male, 57 years). In the frame an enlargement of the cervical myelum and cervical nerve roots is shown.

Figure 3.4 shows an example of the resulting tractography of the cervical spinal cord obtained from the DTI myelum data. The semi-transparent white column represents the automatically selected region of interest (ROI) that serves as seed volume for tractography.

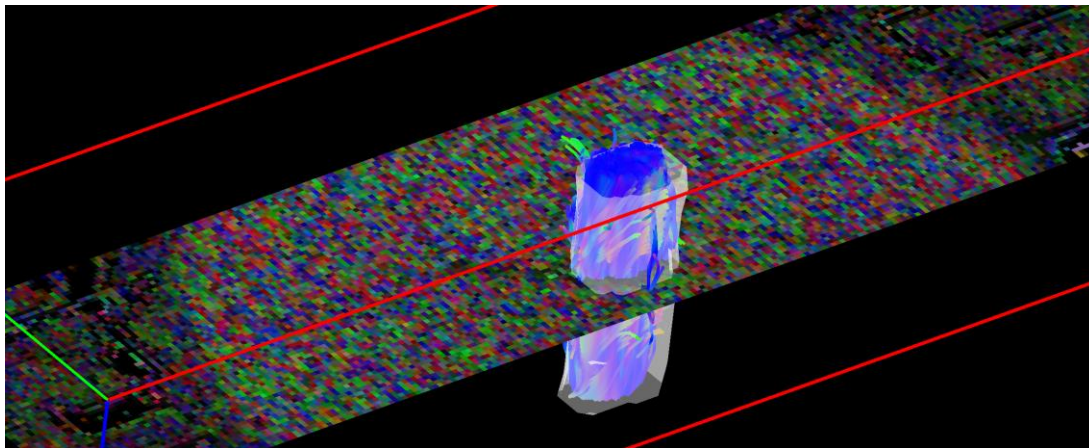


Figure 3.4 Tractography of a cervical spinal cord using automatically selected region of interest (ROI). The automatically selected ROI is shown in white.

In Table 3.2 the calculated diffusion parameters of the spinal cord itself, obtained with the DTI myelum protocol are shown. The results in this table show no significant differences in FA and diffusivity between healthy controls and patients with SMA.

Table 3.2 Diffusion parameters of cervical spinal cord in patients with SMA and healthy controls.

| | FA (mean ± SD) | MD (mean ± SD) | Diffusivity (mm ² /s) × 10 ⁻³ | |
|----------------|----------------|----------------|---|----------------|
| | | | AD (mean ± SD) | RD (mean ± SD) |
| Control | 0.56 ± 0.05 | 0.79 ± 0.15 | 1.36 ± 0.28 | 0.50 ± 0.08 |
| SMA | 0.58 ± 0.03 | 0.84 ± 0.18 | 1.48 ± 0.31 | 0.52 ± 0.11 |

All calculated diffusion parameters of the lower cervical nerves (C5-C7) are shown in Table 3.3. There was a significant difference between patients and healthy controls for FA ($p < 0.05$), MD ($p < 0.005$), AD ($p < 0.005$), and RD ($p < 0.005$).

Table 3.3 Diffusion parameters of lower cervical nerves (C5-C7) in patients with SMA and healthy controls, calculated from the data obtained with the DTI roots sequence.

| | Diffusivity (mm^2/s) $\times 10^{-3}$ | | | |
|----------------|---|--------------------|--------------------|--------------------|
| | FA (mean \pm SD) | MD (mean \pm SD) | AD (mean \pm SD) | RD (mean \pm SD) |
| Control | 0.33 \pm 0.04 [†] | 1.00 \pm 0.17* | 1.37 \pm 0.23* | 0.82 \pm 0.14* |
| SMA | 0.31 \pm 0.04 [†] | 0.82 \pm 0.26* | 1.10 \pm 0.35* | 0.69 \pm 0.22* |

* $p < 0.005$

[†] $p < 0.05$

Table 3.4 specifies the diffusion parameters per nerve level, for C5 to C7. A result of the different tract segments over which diffusion parameters were calculated for a patient and a healthy control is shown in Figure 3.5. The average nerve tract length over which diffusion parameters were calculated was 5.5 slices for healthy controls. For patients the average nerve tract length was 4 slices. For level C5, all diffusion parameters are significantly different. For level C6, significant differences are found in MD and AD. No significant differences are found on nerve level C7.

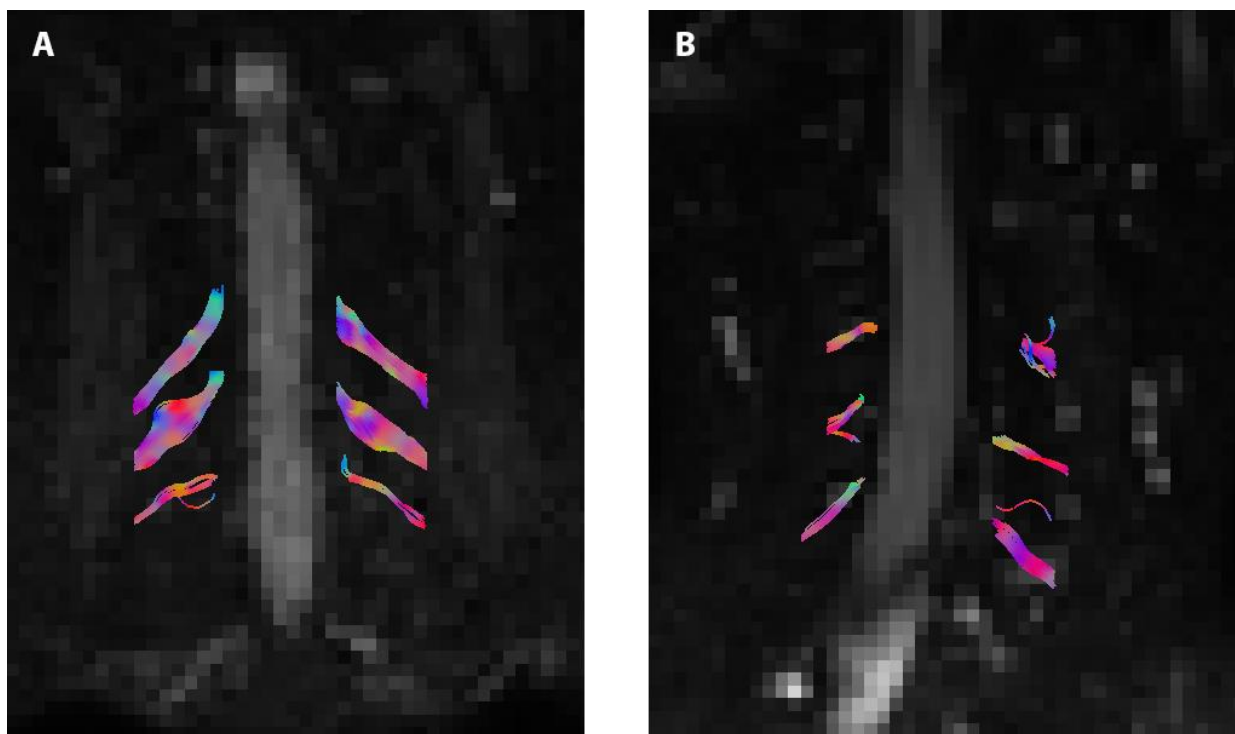


Figure 3.5 Nerve tract segments (C5-C7) over which diffusion parameters are calculated are shown. (A) shows the tract segments in a healthy control and (B) shows the tract segments in an SMA patient.

Table 3.4 Diffusion parameters specified for lower cervical nerves (C5-C7) in patients with SMA and healthy controls, calculated from the data obtained with the DTI roots sequence.

| Nerve | | Diffusivity (mm ² /s) x 10 ⁻³ | | | |
|-------|---------|---|--------------------------|--------------------------|--------------------------|
| | | FA (mean±SD) | MD (mean±SD) | AD (mean±SD) | RD (mean±SD) |
| C5 | Control | 0.34 ± 0.05 [†] | 1.03 ± 0.16* | 1.43 ± 0.20* | 0.83 ± 0.14 [†] |
| | SMA | 0.32 ± 0.06 [†] | 0.83 ± 0.21* | 1.11 ± 0.26* | 0.69 ± 0.19 [†] |
| C6 | Control | 0.34 ± 0.04 | 1.04 ± 0.18 [†] | 1.44 ± 0.23 [†] | 0.84 ± 0.16 |
| | SMA | 0.32 ± 0.04 | 0.85 ± 0.30 [†] | 1.14 ± 0.41 [†] | 0.70 ± 0.24 |
| C7 | Control | 0.30 ± 0.03 | 0.94 ± 0.16 | 1.25 ± 0.20 | 0.78 ± 0.13 |
| | SMA | 0.30 ± 0.03 | 0.80 ± 0.29 | 1.04 ± 0.37 | 0.67 ± 0.24 |

* p < 0.005

[†] p < 0.05

3.4 DISCUSSION

To our knowledge this small scale preliminary study is the first study that investigates anatomical and microstructural properties of the cervical spinal cord and nerves in patients with SMA. We report significant differences between SMA patients and healthy controls in all diffusion parameters of the descending nerve roots (C5-C7). In a case report, differences in anatomy were found in grey matter to spinal cord area ratio and in anterior to posterior nerve root diameter ratio between an SMA patient and a healthy control.

3.4.1 Anatomical measurements

The mFFE images demonstrate a difference between an SMA patient and an age- and gender matched healthy control in grey matter to cervical spinal cord ratio. The main contributor for this difference in ratio is the smaller grey matter area measured in the SMA patient. The pathophysiological mechanisms of SMA explain this finding, since degeneration of alpha motor neurons in the anterior horn of the grey matter in the spinal cord is characterizing SMA.⁴ Another post mortem study of Kumagai et al.⁷⁸ underlines this finding.

Diameter measurements of the nerve roots in the PSIF images show a difference in anterior to posterior nerve root ratio between an SMA patient and an age- and gender matched healthy control. In the patient, a difference in diameter between the anterior and posterior root is measured; the diameter of the anterior nerve root is smaller than that of the posterior nerve root. This difference in diameters is not seen in the healthy control. The most likely cause for this is degeneration of axons. Axonal decrease or axonal loss in the nerve root is a consequence of degeneration of the nucleus in the anterior horn of the spinal cord, a process called Wallerian degeneration.⁷⁹ Several post mortem studies demonstrate axonal loss in SMA patients.⁸⁰⁻⁸³

The results of the anatomical sequences are presented as a case report, because the image quality of the mFFE sequence and the PSIF sequence varied considerably between subjects. As a result, it was impossible to compare more patients directly to their age- and gender matched healthy controls. The difference in image quality was particularly noticeable within the patient group. A possible explanation for the varying quality is subject movement. Fast field echo as well as gradient echo sequences are both rather sensitive to movement^{84,85}, so small movements can easily result in a blurred image.^{86,87} During the development of both sequences movement was not experienced as a problem and sharp images were obtained. However, those experiments were performed on mainly young, healthy subjects. The included SMA patients not only have a wider age range, they often suffer from (disease-related) tremor in the extremities. In electrocardiography it is shown that essential tremor can cause artefacts.⁸⁸⁻⁹⁰ Besides subject movement in general, tremor of the patient could be of extra influence on the image quality.

3.4.2 Tractography

Significant differences between SMA patients and healthy controls were found in all diffusion parameters of the descending nerve roots (C5-C7). The diffusion parameters of the myelum showed no significant differences between patients and healthy controls. A possible explanation for these findings comes from the underlying physiological principle used in DTI, namely diffusion. As mentioned in Chapter 2, diffusion signal is measured according to the rate and direction of diffusion. If diffusion is isotropic the FA will be low; if diffusion is anisotropic the FA will be high.⁶⁶ In the myelum a clear distinction in random motion can be made; in the grey matter mainly cell bodies are present (isotropic diffusion) and in the white matter mainly axons are present (anisotropic diffusion).⁹¹ The pathological principle of SMA originates in the alpha motor neurons of the grey matter.⁴ However, the tractography results of the DTI myelum sequence are based on the tracts in the white matter, which is a combination of healthy sensory axons, healthy motor axons originating from motor neurons other than alpha, and possibly affected axons originating from alpha motor neurons. The proportion of the affected axons is relatively low compared to the non-affected axons. Potential differences due to SMA pathology in the DTI myelum sequence are presumably averaged out. The DTI roots sequence is developed to measure only small segments of the total axon bundle, the cervical nerves. The cervical nerve is a combination of healthy sensory axons and affected motor axons, but the proportion of affected motor axons originating from alpha motor neurons is larger. Therefore it is more likely to measure differences between healthy controls and SMA patients. This is in accordance with the results we found with the DTI roots sequence. The lower diffusion parameters that are found in SMA patients can be explained by cytoskeletal breakdown, which is a process that occurs during axonal loss.⁴² Cytoskeletal breakdown results in increased viscosity of the axons, thereby reducing anisotropic water diffusion in the intra-axonal space.

The aim was to perform tractography over a tract segment length of 6 slices. In patient datasets the average tract segment length that could be selected was lower than in datasets of healthy controls. The difficulties in performing tractography over a tract length of 6 slices can be due to different factors.

First of all, morphology of the descending nerves could have an effect on the diffusion signal, in patients as well as in healthy controls. Sugimoto et al.⁹² report nerve root sizes in healthy subjects of 2.14 ± 0.30 mm for C5, 2.99 ± 0.45 mm for C6, and 3.39 ± 0.48 mm for C7, measured with ultrasonography. The voxel size of the DTI roots sequence is 2.5 mm isotropic. This relatively large voxel size of the acquisition protocol in combination with the small diameter of the imaged nerves could lead to the partial volume effect.^{93,94} The partial volume effect is the loss of contrast between two adjacent tissues in an image caused by insufficient resolution, so that more than one tissue type occupies the same voxel.⁹⁵ In the ideal case, the nerve passes exactly through the center of the voxel, thereby avoiding the partial volume effect. However, in reality it is more likely that the nerve passes through parts of two, or even three or four voxels, leading to the partial volume effect. The course of the nerve contributes to this effect, because if the nerve passes through the matrix diagonally, the anisotropic properties of the nerve are averaged with surrounding voxels with a much lower anisotropy, through which tractography is more difficult to perform.

Secondly, pathology of the patient also influences the diffusion signal. The pathological principal of SMA is degeneration of motor neurons in the spinal cord¹⁰, subsequently leading to fewer axons originating from the spinal cord.⁹⁶ To investigate such pathophysiological mechanisms is one of the aims of this study. However, based on the hypothesis that nerve roots in patients have a slightly smaller diameter than nerve roots in healthy controls, it could be that the partial volume effect has a larger impact on patient data than on healthy control data, resulting in a difference in measured tract length.

Thirdly, the diffusion data might be influenced by motion artefacts. Total scanning time for the DTI roots sequence was 10 minutes and 6 seconds. It is difficult to lie completely still for this length of time, for patients as well as for healthy controls. Besides, anatomical structures such as the lungs and esophagus are in the direct neighborhood of the nerves of interest. The lungs and esophagus are innervated by the autonomic nervous system and therefore the subject does not voluntarily control movement of these organs. Despite the fact that all datasets were corrected for subject motion and eddy current induced distortions^{75,76}, local deformations and nonlinear motion artefacts caused by respiratory and cardiac movement could still be present.⁹⁷

4 CONCLUSION AND FUTURE PERSPECTIVES

4.1 CONCLUSION

This master thesis focused on DTI as an imaging technique to visualize the cervical spinal cord and the descending nerve roots in patients with SMA. The main research questions were: ‘*How can we image the morphology and microstructural properties of the cervical spinal cord and its nerve roots with the use of DTI?*’ and ‘*What is the potential value of DTI as a biomarker for disease severity in SMA patients?*’

We developed, optimized and validated an acquisition protocol and showed that it is possible to visualize the anatomical and microstructural properties of the cervical spinal cord and the descending nerve roots. The acquisition protocol consists of two diffusion weighted acquisition sequences and two T2-weighted acquisition sequences. We used the developed acquisition protocol to perform a clinical study. To our knowledge this was the first clinical study that used DTI to investigate the anatomical and microstructural properties of the cervical spinal cord and nerves in patients with SMA. Preliminary results show significant differences in FA, MD, AD, and RD between SMA patients and healthy controls for nerves C5-C7. Anatomical differences were found in grey matter to spinal cord area ratio and in anterior to posterior nerve root diameter ratio between an SMA patient and a healthy control. DTI can provide additional unique information regarding the pathophysiological mechanisms of SMA *in vivo* and enables new perspectives on the pathophysiological mechanisms of the disease.

This study provides a foundation for further exploration of DTI as a biomarker in SMA. Combining anatomical imaging, DTI and tractography, and correlating diffusion parameters with clinical outcome measures may prove a valuable contribution to better monitor the disease progression and therapeutic effect in SMA patients in the future.

4.2 FUTURE PERSPECTIVES

We believe that DTI can be of clinical added value as a biomarker in SMA patients. Nevertheless before DTI could be actually implemented in clinical practice as a biomarker for disease severity, several steps must be taken.

4.2.1 Protocol optimization

A robust acquisition protocol is essential for acquiring valid data. The developed protocol is robust in the sense that it is able to visualize the anatomical and microstructural properties, but it is quite sensitive to movement. If the amount of motion artefacts can be reduced, more consistent data can be obtained and more valid comparisons can be made. There are different ways to obtain this goal.

First of all, the developed protocol can be further optimized. The mFFE and PSIF sequences we chose for anatomical imaging are known for their sensitivity to movement. During development of the protocol

we experienced no difficulties, so we chose these sequences because of their remarkable distinction between grey and white matter in the spinal cord (mFFE), and their ability to visualize nerve roots originating from the myelum (PSIF). With the knowledge that we have now we can reconsider the anatomical sequences and look into the possibilities of a turbo spin echo (TSE) sequence, which is less sensitive to movement. A TSE sequence was added to the protocol already, so analysis of these results can provide information on a more robust anatomical sequence. In the diffusion sequences, the lack of resolution which causes the partial volume effect appears to be the main contributor to the problem of unstable data. The long acquisition time of the roots sequence causes some difficulties as well. A possible solution for these two problems can be to split the roots acquisition sequence in two different scan packages, so that data of the left and right cervical nerve roots is acquired separately. Advantages of acquiring the information in two different packages are the shorter continuous scanning time and a higher resolution that can be achieved. A disadvantage of splitting the roots acquisition is that the data of left and right can not be directly compared anymore. However, since SMA appears to be a disease in which patients are symmetrically bilateral affected⁹⁸, the advantages probably outweigh the disadvantage.

Secondly, improvements can be made according to the scanning set up. To acquire the data, we used the most dedicated coil available in the clinic, which focusses specifically on the head, neck and spine area. This coil is shaped in such a way that the head is surrounded by a cage structure, and it has an extra slab at the front to cover the anterior neck area. We chose not to fixate the head of the patient during scanning, because we assumed that movement in the coil was quite limited already. However, the resulting images of the sequences showed considerable motion artefacts, so fixating the head of the patient could help to obtain more robust images. Total fixation can be done with a face covering mask that is used in radiotherapy treatment, but this is quite burdensome for the patient. Another option is to use a vacuum mattress, which is specifically designed to immobilize a patient. However, this mattress does not fit in the dedicated coil, so the result would be that the body of the patient is immobilized, but the head could still move freely. A third option can be to use a neck pillow that fills the gaps between the patient and the anterior slab, sides and posterior base of the coil. Regular neck pillows are too large to fit in, but if a smaller neck pillow is designed this can result in better fixation of the patient and thereby fewer motion artefacts.

Another step in the further development of the protocol can be to optimize the roots sequence for imaging other anatomical areas of the patient. The muscles of the lower limbs in SMA patients are weaker than the muscles of the upper limbs⁹⁹, so we hypothesize that the nerves in that area will be more affected as well. Nerves that innervate the lower limbs originate from the cauda equina. These nerves are larger than the cervical nerves, so the influence of the partial volume effect is probably less present. Besides that, fewer artefacts due to subject movement are to be expected because, as opposed to in the neck, the nerves originating from the cauda equina are situated in a more static environment.

4.2.2 Clinical study

To date, nine out of ten patients and eighteen out of twenty healthy controls are included in MuSIC. The first step is to complete inclusion for MuSIC. In a later stadium study extension should be done as well, not only in subject quantity, but also in different disease types. The next step is to expand the analysis of available data. Data analysis was difficult in the current datasets. For the diffusion data this was mainly due to partial volume effect and for the anatomical data this was mainly due to motion artefacts. To improve the quality of the present data, further research in post-processing ‘noise reduction’ methods and motion correction methods can be done.

When a more robust protocol and thus more robust data is available, a broader comparison in grey matter to spinal cord ratio and anterior to posterior nerve root diameter ratio between patients and healthy controls can be made to see if the differences that the case report showed are also present in a larger subject group. Robust data also provides more possibilities for computerizing and automating the analyzing methods. We tried to automate the analysis of the current data, but that was only successful for the myelum sequence. Several segmentation methods can be researched further, to make data analysis as objective as possible.

Besides comparing patients to healthy controls, another important step is to investigate if there is a correlation between diffusion parameters and anatomical data and clinical rating scales in patients. Data of several clinical rating scales is obtained in MuSIC. However, due to varying quality of the data it was difficult to make a comparison yet. When more robust data is available, diffusion parameters can be compared with MRC scores to see if the diffusion parameters reflect the differences in strength. It needs to be taken into account that diffusion parameters are assigned to a specific nerve, and MRC scores are assigned to a certain muscle. The cervical nerve roots branch several times before turning into the actual nerve that innervates the muscle. Before comparing diffusion parameters to MRC scores, clear decisions on where on the nerve tract diffusion parameters are measured should be made, because this could influence the results. Decisions on which nerve roots are responsible for the innervation of which muscles should be made as well. When these choices about innervation and location are made, it would be interesting to look at the FA and AD value and compare this to MRC scores. Compared to other diffusion parameters, AD changes are considered to be more specific to axonal degeneration⁴², which is the case in patients with SMA.

BIBLIOGRAPHY

1. Sugarman, E. a *et al.* Pan-ethnic carrier screening and prenatal diagnosis for spinal muscular atrophy: clinical laboratory analysis of >72 400 specimens. *Eur. J. Hum. Genet.* **20**, 27–32 (2012).
2. Monani, U. R. Spinal muscular atrophy: A deficiency in a ubiquitous protein; a motor neuron-specific disease. *Neuron* **48**, 885–896 (2005).
3. Dubowitz, V. Ramblings in the history of spinal muscular atrophy. *Neuromuscul. Disord.* **19**, 69–73 (2009).
4. Araki, S. *et al.* Neuropathological analysis in spinal muscular atrophy type II. *Acta Neuropathol.* **106**, 441–448 (2003).
5. Munsat, T. L. International SMA Collaboration. *Neuromuscul. Disord.* **1**, 81 (1991).
6. Farrar, M. a., Vucic, S., Johnston, H. M., du Sart, D. & Kiernan, M. C. Pathophysiological Insights Derived by Natural History and Motor Function of Spinal Muscular Atrophy. *J. Pediatr.* 155–159 (2012). doi:10.1016/j.jpeds.2012.05.067
7. Lorson, C. A single nucleotide in the SMN gene regulates splicing and is responsible for spinal muscular atrophy. *Proc. Natl. Acad. Sci. U. S. A.* **96**, 6307–6311 (1999).
8. Humphrey, E., Fuller, H. R. & Morris, G. E. Current research on SMN protein and treatment strategies for spinal muscular atrophy. *Neuromuscul. Disord.* **22**, 193–197 (2012).
9. Li, D. K., Tisdale, S., Lotti, F. & Pellizzoni, L. SMN control of RNP assembly: From post-transcriptional gene regulation to motor neuron disease. *Semin. Cell Dev. Biol.* **32**, 22–29 (2014).
10. Gubitz, A. K., Feng, W. & Dreyfuss, G. The SMN complex. *Exp. Cell Res.* **296**, 51–56 (2004).
11. Terns, M. P. & Terns, R. M. Macromolecular complexes: SMN--the master assembler. *Curr. Biol.* **11**, R862–4 (2001).
12. Burghes, A. H. M. & Beattie, C. E. Spinal muscular atrophy: why do low levels of survival motor neuron protein make motor neurons sick? *Nat. Rev. Neurosci.* **10**, 597–609 (2009).
13. Wirth, B. *et al.* Quantitative analysis of survival motor neuron copies: identification of subtle SMN1 mutations in patients with spinal muscular atrophy, genotype-phenotype correlation, and implications for genetic counseling. *Am. J. Hum. Genet.* **64**, 1340–1356 (1999).
14. Renault, F., Raimbault, J., Praud, J. P. & Laget, P. Electromyographic study of 50 cases of Werdnig-Hoffmann disease. *Rev. Electroencephalogr. Neurophysiol. Clin.* **13**, 301–305 (1983).
15. Chiriboga, C. *et al.* Sensory-Motor Circuit Dysfunction In Adult Ambulatory SMA Type 3 Patients (P4.087). *Neurology* **82**, P4.087 (2014).
16. Schmid, A. & DiDonato, C. J. Animal models of spinal muscular atrophy. *J. Child Neurol.* **22**, 1004–

1012 (2007).

17. Martínez-Hernández, R. *et al.* Synaptic defects in type I spinal muscular atrophy in human development. *J. Pathol.* **229**, 49–61 (2013).
18. Wadman, R. I., Vrancken, A. F. J. E., Van Den Berg, L. H. & Van Der Pol, W. L. Dysfunction of the neuromuscular junction in spinal muscular atrophy types 2 and 3. *Neurology* **79**, 2050–2055 (2012).
19. Main, M., Kairon, H., Mercuri, E. & Muntoni, F. The Hammersmith functional motor scale for children with spinal muscular atrophy: A scale to test ability and monitor progress in children with limited ambulation. *Eur. J. Paediatr. Neurol.* **7**, 155–159 (2003).
20. O'Hagen, J. M. *et al.* An expanded version of the Hammersmith Functional Motor Scale for SMA II and III patients. *Neuromuscul. Disord.* **17**, 693–697 (2007).
21. Glanzman, A. M. *et al.* Validation of the Expanded Hammersmith Functional Motor Scale in Spinal Muscular Atrophy Type II and III. *J. Child Neurol.* **26**, 1499–1507 (2011).
22. Bérard, C., Payan, C., Hodgkinson, I., Fermanian, J. & The MFM Collaborative Study Group. A motor function measure scale for neuromuscular diseases. Construction and validation study. *Neuromuscul. Disord.* **15**, 463–470 (2005).
23. Vuillerot, C., Payan, C., Iwaz, J., Ecochard, R. & Bérard, C. Responsiveness of the motor function measure in patients with spinal muscular atrophy. *Arch. Phys. Med. Rehabil.* **94**, 1555–61 (2013).
24. Montes, J., Gordon, A. M., Pandya, S., De Vivo, D. C. & Kaufmann, P. Clinical outcome measures in spinal muscular atrophy. *J. Child Neurol.* **24**, 968–978 (2009).
25. van der Ploeg, R. J., Oosterhuis, H. J. & Reuvekamp, J. Measuring muscle strength. *J. Neurol.* **231**, 200–203 (1984).
26. Clark, C. a. & Werring, D. J. Diffusion tensor imaging in spinal cord: Methods and applications - A review. *NMR Biomed.* **15**, 578–586 (2002).
27. Maier, S. E. & Mamata, H. Diffusion tensor imaging of the spinal cord. *Ann. N. Y. Acad. Sci.* **1064**, 50–60 (2005).
28. Maier, S. E. Examination of Spinal Cord Tissue Architecture with Magnetic Resonance Diffusion Tensor Imaging. *Neurotherapeutics* **4**, 453–459 (2007).
29. Ellingson, B. M., Ulmer, J. L., Kurpad, S. N. & Schmit, B. D. Diffusion tensor MR imaging of the neurologically intact human spinal cord. *AJNR. Am. J. Neuroradiol.* **29**, 1279–1284 (2008).
30. Onu, M. *et al.* Human cervical spinal cord funiculi: Investigation with magnetic resonance diffusion tensor imaging. *J. Magn. Reson. Imaging* **31**, 829–837 (2010).
31. Lindberg, P. G., Feydy, A. & Maier, M. a. White matter organization in cervical spinal cord relates differently to age and control of grip force in healthy subjects. *J. Neurosci.* **30**, 4102–4109 (2010).

32. Barakat, N. *et al.* Diffusion tensor imaging of the normal pediatric spinal cord using an inner field of view echo-planar imaging sequence. *Am. J. Neuroradiol.* **33**, 1127–1133 (2012).
33. Mezzapesa, D. M. *et al.* A preliminary diffusion tensor and magnetization transfer magnetic resonance imaging study of early-onset multiple sclerosis. *Arch. Neurol.* **61**, 366–368 (2004).
34. Valsasina, P. *et al.* Mean diffusivity and fractional anisotropy histogram analysis of the cervical cord in MS patients. *Neuroimage* **26**, 822–828 (2005).
35. Agosta, F. *et al.* In vivo assessment of cervical cord damage in MS patients: A longitudinal diffusion tensor MRI study. *Brain* **130**, 2211–2219 (2007).
36. Oh, J. *et al.* Spinal cord quantitative MRI discriminates between disability levels in multiple sclerosis. *Neurology* **80**, 540–7 (2013).
37. Valsasina, P. *et al.* Diffusion anisotropy of the cervical cord is strictly associated with disability in amyotrophic lateral sclerosis. *J. Neurol. Neurosurg. Psychiatry* **78**, 480–484 (2007).
38. Philips. *Basic principles of MR imaging.* (2010).
39. Eom, H. J. in *Prim. Theory Electromagn.* 95–111 (2013). doi:10.1007/978-94-007-7143-7
40. Le Bihan, D. *et al.* Diffusion tensor imaging: concepts and applications. *J. Magn. Reson. Imaging* **13**, 534–46 (2001).
41. Basser, P. J., Mattiello, J. & LeBihan, D. MR diffusion tensor spectroscopy and imaging. *Biophys. J.* **66**, 259–267 (1994).
42. Beaulieu, C. The basis of anisotropic water diffusion in the nervous system - A technical review. *NMR Biomed.* **15**, 435–455 (2002).
43. Tuch, D. S. Diffusion MRI of Complex Tissue Structure. *Science (80-.)*. 220 (2002).
44. Froeling, M. Diffusion tensor imaging of human skeletal muscle: from simulation to clinical implementation. (2012). doi:http://dx.doi.org/10.6100/IR737539
45. Dougherty, G. Image analysis in medical imaging: recent advances in selected examples. *Biomed. Imaging Interv. J.* **6**, (2010).
46. Pierpaoli, C. & Basser, P. J. Toward a quantitative assessment of diffusion anisotropy. *Magn. Reson. Med.* **36**, 893–906 (1996).
47. Basser, P. J. & Pierpaoli, C. Microstructural and physiological features of tissues elucidated by quantitative-diffusion-tensor MRI. 1996. *J. Magn. Reson.* **213**, 560–70 (2011).
48. Pajevic, S. & Pierpaoli, C. Color schemes to represent the orientation of anisotropic tissues from diffusion tensor data: Application to white matter fiber tract mapping in the human brain. *Magn. Reson. Med.* **42**, 526–540 (1999).

49. Mori, S. & Zhang, J. Principles of Diffusion Tensor Imaging and Its Applications to Basic Neuroscience Research. *Neuron* **51**, 527–539 (2006).
50. Mori, S. & van Zijl, P. C. M. Fiber tracking: principles and strategies - a technical review. *NMR Biomed.* **15**, 468–480 (2002).
51. Brix, G. *et al.* in *Magn. Reson. Tomogr.* (Reiser, M., Semmler, W. & Hricak, H.) 3–167 (Springer Berlin Heidelberg, 2008). doi:10.1007/978-3-540-29355-2_2
52. Oudeman, J. *et al.* Techniques and applications of skeletal muscle diffusion tensor imaging: A review. *J. Magn. Reson. Imaging* n/a–n/a (2015). doi:10.1002/jmri.25016
53. Sexton, C. E., Mackay, C. E. & Ebmeier, K. P. A Systematic Review of Diffusion Tensor Imaging Studies in Affective Disorders. *Biol. Psychiatry* **66**, 814–823 (2009).
54. van Ewijk, H., Heslenfeld, D. J., Zwiers, M. P., Buitelaar, J. K. & Oosterlaan, J. Diffusion tensor imaging in attention deficit/hyperactivity disorder: A systematic review and meta-analysis. *Neurosci. Biobehav. Rev.* **36**, 1093–1106 (2012).
55. Szmuda, M. *et al.* Diffusion tensor tractography imaging in pediatric epilepsy – A systematic review. *Neurol. Neurochir. Pol.* 2–7 (2015). doi:10.1016/j.pjnns.2015.10.003
56. Piper, R. J., Yoong, M. M., Kandasamy, J. & Chin, R. F. Application of diffusion tensor imaging and tractography of the optic radiation in anterior temporal lobe resection for epilepsy: a systematic review. *Clin. Neurol. Neurosurg.* **124**, 59–65 (2014).
57. Otte, W. M. *et al.* A meta-analysis of white matter changes in temporal lobe epilepsy as studied with diffusion tensor imaging. *Epilepsia* **53**, 659–667 (2012).
58. Nair, G. *et al.* Diffusion tensor imaging reveals regional differences in the cervical spinal cord in amyotrophic lateral sclerosis. *Neuroimage* **53**, 576–583 (2010).
59. Wang, Y. *et al.* Preliminary study on cervical spinal cord in patients with amyotrophic lateral sclerosis using MR diffusion tensor imaging. *Acad. Radiol.* **21**, 590–596 (2014).
60. Agosta, F. *et al.* A longitudinal diffusion tensor MRI study of the cervical cord and brain in amyotrophic lateral sclerosis patients. *J. Neurol. Neurosurg. Psychiatry* **80**, 53–55 (2009).
61. Freund, P. *et al.* Recovery after spinal cord relapse in multiple sclerosis is predicted by radial diffusivity. *Mult. Scler.* **16**, 1193–1202 (2010).
62. Miraldi, F., Lopes, F. C., Costa, J. V, Alves-Leon, S. V & Gasparetto, E. L. Diffusion tensor magnetic resonance imaging may show abnormalities in the normal-appearing cervical spinal cord from patients with multiple sclerosis. *Arq. Neuropsiquiatr.* **71**, 580–583 (2013).
63. Cruz, L. C. H., Domingues, R. C. & Gasparetto, E. L. Diffusion tensor imaging of the cervical spinal cord of patients with relapsing-remising multiple sclerosis: a study of 41 cases. *Arq. Neuropsiquiatr.* **67**, 391–395 (2009).

64. Qian, W. *et al.* Quantitative assessment of the cervical spinal cord damage in neuromyelitis optica using diffusion tensor imaging at 3 Tesla. *J. Magn. Reson. Imaging* **33**, 1312–1320 (2011).
65. Rivero, R. L. M. *et al.* Diffusion tensor imaging of the cervical spinal cord of patients with Neuromyelitis Optica. *Magn. Reson. Imaging* **32**, 457–463 (2014).
66. Mukherjee, P., Berman, J. I., Chung, S. W., Hess, C. P. & Henry, R. G. Diffusion Tensor MR Imaging and Fiber Tractography: Theoretic Underpinnings. *Am. J. Neuroradiol.* **29**, 632–641 (2008).
67. Brown, R. W., Cheng, Y.-C. N., Haacke, E. M., Thompson, M. R. & Venkatesan, R. *Magnetic Resonance Imaging: Physical Principles and Sequence Design.* (2014). at <<https://books.google.com/books?hl=en&lr=&id=rQGCAwAAQBAJ&pgis=1>>
68. Lunn, M. & Wang, C. Spinal muscular atrophy. *Lancet* **371**, 2120–33 (2008).
69. Zerres, K. & Davies, K. 59th ENMC International Workshop: Spinal Muscular Atrophies: recent progress and revised diagnostic criteria 17–19 April 1998, Soestduinen, The Netherlands. *Neuromuscul. Disord.* **9**, 272–278 (1999).
70. Miller, R. G. *et al.* A placebo-controlled trial of gabapentin in spinal muscular atrophy. *J. Neurol. Sci.* **191**, 127–131 (2001).
71. Elsheikh, B. *et al.* An analysis of disease severity based on SMN2 copy number in adults with spinal muscular atrophy. *Muscle and Nerve* **40**, 652–656 (2009).
72. Iannaccone, S. T. Outcome measures for pediatric spinal muscular atrophy. *Arch. Neurol.* **59**, 1445–1450 (2002).
73. Merlini, L., Mazzone, E. S., Solari, A. & Morandi, L. Reliability of hand-held dynamometry in spinal muscular atrophy. *Muscle and Nerve* **26**, 64–70 (2002).
74. Leemans, A., Jeurissen, B., Sijbers, J. & Jones, D. ExploreDTI: a graphical toolbox for processing, analyzing, and visualizing diffusion MR data. *Proc. 17th Sci. Meet. Int. Soc. Magn. Reson. Med.* **17**, 3537 (2009).
75. Leemans, A. & Jones, D. K. The *B*-matrix must be rotated when correcting for subject motion in DTI data. *Magn. Reson. Med.* **61**, 1336–1349 (2009).
76. Irfanoglu, M. O., Walker, L., Sarlls, J., Marengo, S. & Pierpaoli, C. Effects of image distortions originating from susceptibility variations and concomitant fields on diffusion MRI tractography results. *Neuroimage* **61**, 275–88 (2012).
77. Veraart, J., Sijbers, J., Sunaert, S., Leemans, A. & Jeurissen, B. Weighted linear least squares estimation of diffusion MRI parameters: Strengths, limitations, and pitfalls. *Neuroimage* **81**, 335–346 (2013).
78. Kumagai, T. & Hashizume, Y. Morphological and Morphometric Studies on the Spinal-Cord Lesion in Werdnig-Hoffmann Disease. *Brain Dev.* **4**, 87–96 (1982).

79. Critchley, E. & Eisen, A. A. *Spinal Cord Disease: Basic Science, Diagnosis and Management*. (Springer Science & Business Media, 2012).
80. Ghatak, N. Spinal roots in Werdnig-Hoffmann disease. *Acta Neuropathol.* **41**, 1–7 (1978).
81. Ikuta, F., Ohama, E., Nakanishi, T., Mannen, T. & Toyokura, Y. Postmortem findings in a case of KW disease; presence of underdeveloped Schwann cells and axons. *Amyotroph. lateral sclerosis. Univ. Tokyo Press. Tokyo* 277–284 (1979).
82. Chien, Y. Y. & Nonaka, I. Peripheral nerve involvement in Werdnig-Hoffmann disease. *Brain Dev.* **11**, 221–229 (1989).
83. Kuru, S. *et al.* An autopsy case of spinal muscular atrophy type III (Kugelberg-Welander disease). *Neuropathology* **29**, 63–7 (2009).
84. Xiao, L. *et al.* MRI of the cervical spine with 3D gradient echo sequence at 3 T: initial experience. *Clin. Radiol.* **70**, 926–931 (2015).
85. van der Meulen, P., Groen, J. P., Tinus, A. M. & Bruntink, G. Fast Field Echo imaging: an overview and contrast calculations. *Magn. Reson. Imaging* **6**, 355–368 (1988).
86. Vargas, M. I., Delavelle, J., Kohler, R., Becker, C. D. & Lovblad, K. Brain and spine MRI artifacts at 3 Tesla. *J. Neuroradiol.* **36**, 74–81 (2009).
87. Dietrich, O., Reiser, M. F. & Schoenberg, S. O. Artifacts in 3-T MRI: Physical background and reduction strategies. *Eur. J. Radiol.* **65**, 29–35 (2008).
88. Robottom, B. J. & Weiner, W. J. Teaching neuroImages: Rest tremor mimicking ventricular tachycardia. *Neurology* **75**, 2134 (2010).
89. Littmann, L. Fact or artifact? The electrocardiographic diagnosis of orthostatic tremor. *J. Electrocardiol.* **43**, 270–3 (2010).
90. Martens, P. & Sinnaeve, P. Tremor mimicking ventricular tachycardia. *Can. Med. Assoc. J.* **187**, E326 (2015).
91. Rossi, C. *et al.* Water diffusion anisotropy in white and gray matter of the human spinal cord. *J. Magn. Reson. Imaging* **27**, 476–482 (2008).
92. Sugimoto, T. *et al.* Ultrasonographic reference sizes of the median and ulnar nerves and the cervical nerve roots in healthy Japanese adults. *Ultrasound Med. Biol.* **39**, 1560–1570 (2013).
93. Alexander, a L., Hasan, K. M., Lazar, M., Tsuruda, J. S. & Parker, D. L. Analysis of partial volume effects in diffusion-tensor MRI. *Magn. Reson. Med.* **45**, 770–780 (2001).
94. Vos, S. B., Jones, D. K., Viergever, M. a. & Leemans, A. Partial volume effect as a hidden covariate in DTI analyses. *Neuroimage* **55**, 1566–1576 (2011).
95. Bankman, I. in *Handb. Med. image Process. Anal.* 1000 (Academic Press, 2008).

96. Markowitz, J. a., Singh, P. & Darras, B. T. Spinal Muscular Atrophy: A Clinical and Research Update. *Pediatr. Neurol.* **46**, 1–12 (2012).
97. Tournier, J.-D., Mori, S. & Leemans, A. Diffusion tensor imaging and beyond. *Magn. Reson. Med.* **65**, 1532–1556 (2011).
98. Wang, C. H. *et al.* Consensus statement for standard of care in spinal muscular atrophy. *J. Child Neurol.* **22**, 1027–49 (2007).
99. ENMC. International sma consortium meeting (26–28 June 1992, Bonn, Germany). *Neuromuscul. Disord.* **2**, 423–428 (1993).

APPENDIX A. APPROVAL MEDICAL ETHICAL COMMITTEE OF STUDY 'MR IMAGING OF THE SPINAL CORD IN PATIENTS WITH SPINAL MUSCULAR ATROPHY (SMA) AND HEALTHY CONTROLS (MUSIC STUDY)'



ALCHER UMCU
2015-05-21
D-15-021371



UMC Utrecht

Medisch Ethische Toetsingscommissie

Divisie Beeld
Afdeling Radiologie
t.a.v. Drs. W. Haakma
Huispost : E01.132

Mw. Drs. M.D. van de Loo-Waller
Telefoon 088-7556376 (na 17m do)
Heidelberglaan 100
Postbus 85500
3508 GA Utrecht
Huispost D 01.343
E-mail metc@umcutrecht.nl
Info www.umcutrecht.nl/metc

Datum
13 mei 2015
Onderwerp
METC-protocolnummer 15-161/M
NL52615.041.15, versie 02
Besluit positief monocenter

Ons kenmerk
MvdL/om/15/021371
Uw kenmerk

Geachte heer/mevrouw Haakma,

De Medisch Ethische Toetsingscommissie (METC), erkend op 11 november 1999 ex artikel 16 van de WMO heeft zich in de vergadering van 05 mei 2015 beraden over het onderzoeksvoorstel nummer 15/161, getiteld "**MR imaging of the spinal cord in patients with spinal muscular atrophy (SMA) and healthy controls (MUSIC study)**", ingediend door Dr. J. Hendrikse te Utrecht, met als verrichter UMC Utrecht te Utrecht.

De commissie heeft als door de CCMO erkende METC bij de vorming van haar oordeel de door u voorgelegde documenten getoetst aan de criteria en randvoorwaarden, zoals deze zijn vastgelegd in de WMO, alsmede in het ICH-Richtsoer voor GCP en andere relevante Nederlandse en/of Europese regelgeving, en zij heeft zich beraden over de geschiktheid van het protocol, terzake de doelstelling en de reden van het onderzoek, de opzet van het onderzoek, de ethische aspecten, de methoden en het materiaal dat zal worden gebruikt om het informed consent van de proefpersonen te verkrijgen en te documenteren.

De commissie komt tot het oordeel dat de rechten, de veiligheid en het welzijn van de proefpersonen in het onderzoek worden beschermd en geeft op basis van haar bevoegdheid wegens art. 2, tweede lid, onder a van de WMO, met inachtneming van artikel 3 van de WMO, een positief oordeel dit onderzoek uit te voeren.

De commissie is van oordeel dat:

- de te verwachten wetenschappelijke opbrengst van het onderzoek de belasting voor de proefpersonen rechtvaardigt;
- met de uitvoering van het onderzoeksprotocol niet in strijd wordt gehandeld met de verboden als weergegeven in de artikelen 4, eerste lid, 5 en 6, eerste lid van de WMO;
- gelet op het bepaalde in artikel 6, derde t/m zevende lid, van de WMO, de proefpersonen op adequate, volledige en begrijpelijke wijze worden geïnformeerd;

De commissie heeft voorts vastgesteld dat op correcte wijze uitvoering is gegeven aan de verzekeringsplicht als neergelegd in artikel 7 van de WMO, zoals nader uitgewerkt in het

Besluit verplichte verzekering bij medisch-wetenschappelijk onderzoek met mensen (besluit van 23 juni 2003, Stb. 2003, 266). In het geval het verzekeringscertificaat tijdens de voortgang van het onderzoek zijn geldigheid verliest, dient aan de METC tijdig een afschrift van een nieuw geldig certificaat te worden toegestuurd. De commissie wijst u er op dat sinds 1 maart 2006 daarnaast de aansprakelijkheid van de verrichter of de uitvoerder(s) gedekt moet zijn voordat met de uitvoering van het onderzoek wordt gestart. Een bestaande aansprakelijkheidsverzekering daartoe is voldoende.

- De commissie dient (eventueel per E-mail) op de hoogte te worden gesteld van de definitieve startdatum van het onderzoek. Dat is de datum waarop de inclusie van de eerste proefpersoon plaatsvindt;
- De commissie wil over een jaar en ieder jaar daaropvolgend over de voortgang van het onderzoek worden geïnformeerd. U kunt hiervoor het formulier voortgangsrapportage gebruiken, dat te vinden is op de in het briefhoofd genoemde site.
- De onderzoeker dient de commissie er door middel van het formulier "melding beëindiging studie" van op de hoogte te stellen wanneer het onderzoek afgerond is (dit is het moment waarop de laatste meting bij de laatste proefpersoon is uitgevoerd);
- Binnen één jaar na afronding van het onderzoek dient de commissie een eindrapportage te ontvangen, met eventuele publicaties / abstracts.
- Iedere wijziging (amendement) van het protocol, hoe ogenschijnlijk gering ook, dient u opnieuw voor toestemming aan de METC voor te leggen.
- Het positief oordeel verliest zijn geldigheid als met het uitvoeren van het onderzoek niet is begonnen binnen een jaar nadat dit besluit is genomen.

De volgende gebeurtenissen dienen onmiddellijk te worden gemeld:

- Indien het onderzoek voortijdig wordt beëindigd is het de plicht van de hoofdonderzoeker, en indien van toepassing van de sponsor, om de stopzetting van dit onderzoek in het UMC Utrecht te melden bij de METC, met opgave van redenen;
- Wanneer zich een ernstige onverwachte bijwerking of een ernstig ongewenst voorval voordoet, of wanneer het verloop binnen het onderzoek in noemenswaardige mate ongunstiger is dan in het protocol is voorzien (art 10 van de WMO), dient u de METC hiervan eveneens op de hoogte te stellen. Zie voor de regels rond het melden van de SUSAR's en SAE's: www.ccmo.nl;
- Nieuwe informatie die ongunstige consequenties heeft voor de veiligheid van de proefpersoon of de uitvoering van het klinisch onderzoek;

Volledigheidshalve wil de commissie u erop wijzen dat de uitvoering van het onderzoek niet eerder gestart mag worden dan nadat daartoe toestemming van de raad van bestuur of directie van de instelling is verkregen. De toestemming van de Raad van Bestuur van het UMC Utrecht voor de uitvoering in het UMC Utrecht volgt doorgaans spoedig na ontvangst van het positieve oordeel.

Ingevolge artikel 23 van de WMO kan degene wiens belang rechtstreeks bij dit besluit betrokken is, binnen zes weken na dagtekening van dit besluit een beroepschrift indienen bij de Centrale Commissie Mensgebonden Onderzoek (CCMO). Een dergelijk beroepschrift dient u te adresseren aan: CCMO, postbus 16302, 2500 BH Den Haag.



The Medical Research Ethics Committee (METC) of the University Medical Center Utrecht confirms that it has reviewed the research in accordance with the Dutch Medical Research Involving Human Subjects Act (WMO) and other applicable Dutch and European regulations. The METC of the University Medical Center Utrecht has granted a positive judgement based on Article 2 and 3 of the WMO.

Met vriendelijke groeten,
namens de METC,

b.a.

Drs. M.D. van de Loo-Waller
Secretaris METC

De commissie heeft in haar vergadering de beschikking gehad over de volgende documenten:

| Naam | Datum Ontvangst |
|--|--------------------|
| A1. Reactiebrief indiener d.d. 28-04-2015 met beantwoording vragen.pdf | 6-5-2015 |
| A1. Reactiebrief indiener dd 28-04-2015.pdf | 30-4-2015 |
| A1. Aanbiedingsbrief dd 27-02-2015.pdf | 9-3-2015 |
| B1. ABR-formulier versie 2 dd 28-04-2015.pdf | 30-4-2015 |
| C1. Onderzoeksprotocol versie 2, april 2015.pdf | 30-4-2015 |
| C1. Protocol Signature Sheet versie 2.pdf | 30-4-2015 |
| E1. + E2. Informatie en toestemmingsformulier controles 12tot18jr versie 2.pdf | 30-4-2015 |
| E1. + E2. Informatie en toestemmingsformulier controles ouders versie 2.pdf | 30-4-2015 |
| E1. + E2. Informatie en toestemmingsformulier controles volwassen versie 2.pdf | 30-4-2015 |
| E1. + E2. Informatie en toestemmingsformulier patient 12tot18jr versie 2.pdf | 30-4-2015 |
| E1. + E2. Informatie en toestemmingsformulier patient ouders versie 2.pdf | 30-4-2015 |
| E1. + E2. Informatie en toestemmingsformulier patient volwassen versie 2.pdf | 30-4-2015 |
| E3. Aanmeldformulier MuSIC study versie 1.0.pdf | 9-3-2015 |
| E3. Begeleidend schrijven bij Informatiebrief versie 1.0.pdf | 9-3-2015 |
| E3. Wervingsbrief controles versie 1.0.pdf | 9-3-2015 |
| E4. Overige informatiemateriaal Informatiefolder MRI.pdf | 9-3-2015 |
| E4. Overige informatiemateriaal Vragenlijst MRI.pdf | 9-3-2015 |
| F1. HFMSSE vragenlijst versie 1.0.pdf | 9-3-2015 |
| F1. Intakeformulier versie 1.0.pdf | 9-3-2015 |
| F1. MFM vragenlijst 1.0.pdf | 9-3-2015 |
| F1. SMA FRS vragenlijst versie 1.0.pdf | 9-3-2015 |

Ons kenmerk
MvdL/om/15/021371

Blad
4 van 4

| | |
|---|----------|
| F1. Telefonisch Screeningsformulier versie 1.0.pdf | 9-3-2015 |
| H1. CV Onafh. deskundige H.S. Goedee dd. 02-02-2015.pdf | 9-3-2015 |
| H2. CV hoofdonderzoeker J. Hendrikse dd. 09-02-2015.pdf | 9-3-2015 |
| K6. Intentieverklaring Neurologie.pdf | 9-3-2015 |
| K6. Monitoringplan versie 1.0.pdf | 9-3-2015 |

cc: CCMO

bijlage: toestemming RvB

Een lijst van de samenstelling van de commissie en het reglement van de commissie zijn op te vragen bij het secretariaat van de METC.